

THESIS

1
2005
62215916

This is to certify that the
thesis entitled

THE ELECTROCHEMICAL OXIDATION AND
AMPEROMETRIC DETECTION OF CATECHOLS AND
CATECHOLAMINES AT BORON-DOPED DIAMOND THIN-
FILM ELECTRODES

presented by

GLORIA FE M. PIMIENTA

has been accepted towards fulfillment
of the requirements for the

M.S. degree in Chemistry

J. M. Swain
Major Professor's Signature

12-16-04

Date

PLACE IN RETURN BOX to remove this checkout from your record.
TO AVOID FINES return on or before date due.
MAY BE RECALLED with earlier due date if requested.

DATE DUE	DATE DUE	DATE DUE

**THE ELECTROCHEMICAL OXIDATION AND AMPEROMETRIC
DETECTION OF CATECHOLS AND CATECHOLAMINES AT
BORON-DOPED DIAMOND THIN-FILM ELECTRODES**

By

Gloria Fe M. Pimienta

A THESIS

**Submitted to
Michigan State University
in partial fulfillment of the requirements
for the degree of**

MASTER OF SCIENCE

Department of Chemistry

2004

ABSTRACT

THE ELECTROCHEMICAL OXIDATION AND AMPEROMETRIC DETECTION OF CATECHOLS AND CATECHOLAMINES AT BORON-DOPED DIAMOND THIN FILM ELECTRODES

By

Gloria Fe M. Pimienta

The electrochemical oxidation and amperometric detection of catechols and catecholamines were investigated using the new electrode material, diamond thin film. The films were synthesized by chemical vapor deposition and made electrically conducting by doping with boron. In general, diamond has properties superior to those of other commonly used sp^2 carbon electrodes (e.g., glassy carbon), among which are low background current, good response precision, stable response without pretreatment, and high resistance to fouling. Cyclic voltammetric investigations were carried out to evaluate the electrode response for dopamine, catechol, and 3,4-dihydroxyphenylacetic acid as a function of the potential sweep rate and solution pH. The electrode performance for the amperometric detection of these and other catecholamines in flow injection analysis (FIA) and high performance liquid chromatography (HPLC) was evaluated in terms of linear dynamic range, limit of quantitation, sensitivity, and response precision. The mass limits of quantitation ($S/N > 3$) were 10 – 70 pg in FIA and 10 – 1200 pg in HPLC. The detection figures of merit for untreated diamond are comparable to those for glassy carbon. However, diamond outperformed glassy carbon in terms of response stability and resistance to fouling. Finally, the bioanalytical applicability of the HPLC-EC assay was demonstrated.

To Ian and Angelo

ACKNOWLEDGMENTS

My deepest gratitude goes out to those who have played a vital role in this research, my graduate studies, and my life:

Dr. Greg Swain, my research advisor, for the guidance, encouragement and inspiration that made me do my best and for the support in my research and non-research concerns;

NIH, for the generous funding of the research;

Dr. McGuffin, Dr. Blanchard, Dr. Garrett, and Dr. Galligan, my advisorial committee, for their critical insights that contributed to my accomplishments as a graduate student;

Dr. Show, for the diamond electrodes and for the troubleshooting pointers;

Dr. Lookingland, for the rat plasma samples and for the assistance in the analysis of the results; and his students Troy and Bahareh, for the unselfish help;

Maggie, Matt, Jian, Shannon, Josef, Zuzana, Veronika, Jason S., Perna, Grace, Jason B., Jin Woo, Anne, Doug, Yang, Elizabeth, Wang, and Audrey, my groupmates, for the discussions that made electrochemistry more comprehensible and for the companionship that made the lab a fun place to be in;

MSU Filipino Club, for the Philippine spirit and camaraderie;

Mariano and Pimienta families, for the values that made me the person that I am;

My husband Ian and my baby Angelo, for their love and affection and for the joy that they bring to my heart;

And God Almighty, my provider, for everything that He has blessed me with.

TABLE OF CONTENTS

LIST OF TABLES	vi
LIST OF FIGURES	vii
Chapter 1: INTRODUCTION	1
Chapter 2: EXPERIMENTAL METHODS	12
2.1. Boron-Doped Diamond Thin Film Growth	12
2.2. Boron-Doped Diamond Thin Film Characterization	13
2.2.1. Atomic Force Microscopy	13
2.2.2. X-ray Diffraction	14
2.2.3. Raman Spectroscopy	16
2.2.4. Contact Angle Measurement	18
2.2.5. Cyclic Voltammetry	19
2.3. Glassy Carbon Polishing Procedure	21
2.4. Flow Injection Analysis	21
2.5. High Performance Liquid Chromatography	23
2.6. Chemicals and Reagents	23
Chapter 3: BORON-DOPED DIAMOND THIN-FILM ELECTRODES FOR THE ELECTROCHEMICAL DETECTION OF CATECHOLS AND CATECHOLAMINES	25
3.1. Cyclic Voltammetric Behavior of Catechols and Catecholamines	25
3.1.1. Introduction	25
3.1.2. Results and Discussion	27
3.2. Amperometric Detection of Catechols and Catecholamines in Flow Injection Analysis	43
3.2.1. Introduction	43
3.2.2. Results and Discussion	46
3.3. Conclusions	59
Chapter 4: REVERSED-PHASE HPLC SEPARATION AND AMPEROMETRIC DETECTION OF CATECHOLAMINES AND METABOLITES AT BORON- DOPED DIAMOND THIN-FILM ELECTRODES	62
4.1. Introduction	62
4.2. Results and Discussion	65
4.3. Conclusions	73
Chapter 5: SUMMARY AND CONCLUSIONS	75
BIBLIOGRAPHY	78

LIST OF TABLES

Table 1.1. Detection limits for the catecholamines with ultraviolet, fluorescence and EC detection. ⁶	2
Table 1.2. Molecular structure, pK_a ³⁵ and formula mass of the analytes.	10
Table 2.1. Cyclic voltammetric data for the redox test systems at a microcrystalline diamond thin-film electrode.	21
Table 3.1. ΔE_p values of the catechol compounds at pH 7 for the three electrode types	40
Table 3.2. Reproducibility of the cyclic voltammetric measurements using the three electrode types being studied ($n = 3$).	43
Table 3.3. E_{det} and $E_{1/2}$ values for the amperometric detection of the analytes at microcrystalline diamond, nanocrystalline diamond, and GC.	51
Table 3.4. Response precision (% RSD) for catechol and catecholamine detection at microcrystalline diamond, nanocrystalline diamond, and GC in 0.1 M phosphate buffer, 0.1 M NaCl, pH 7.2.	53
Table 3.5. FIA-EC data for catechol and catecholamine detection at microcrystalline diamond, nanocrystalline diamond, and GC electrodes.	56
Table 4.1. Recent publications on HPLC-EC analysis of catecholamines and metabolites.	64
Table 4.2. Amperometric detection figures of merit for the HPLC-EC analysis of catecholamines and metabolites at nanocrystalline and microcrystalline diamond thin-film electrodes.	69

LIST OF FIGURES

Figure 1.1. The catechol/orthoquinone redox reaction.	3
Figure 1.2. Representative functional groups that might exist on oxidized sp ² carbon surfaces.	4
Figure 1.3. The cubic diamond crystal lattice.	5
Figure 1.4. Background cyclic voltammetric i-E curves in 1.0 M KCl for a microcrystalline diamond film. Scan rate = 100 mV/s. Electrode geometric area = 0.16 cm ²	8
Figure 2.1. AFM images (contact mode, air) of a (A) microcrystalline and (B) nanocrystalline diamond thin film.	14
Figure 2.2. XRD pattern for a (A) microcrystalline and (B) nanocrystalline diamond thin film.	15
Figure 2.3. Visible Raman spectra for a (A) microcrystalline and (B) nanocrystalline diamond thin film. λ _{ex} = 532 nm. Laser power = 30 mW. Integration time = 10 s.	17
Figure 2.4. Diagram of the single compartment, glass electrochemical cell.	19
Figure 2.5. Cyclic voltammetric i-E curves for (A) 1.0 mM Fe(CN) ₆ ^{3-/4-} and (B) 1.0 mM Ru(NH ₃) ₆ ^{3+/2+} at a microcrystalline diamond thin film. The supporting electrolyte was 1.0 M KCl. Scan rate = 100 mV/s. Electrode geometric area = 0.16 cm ²	20
Figure 2.6. Block diagram of the FIA system.	22
Figure 2.7. Schematic of the thin-layer flow cell.	22
Figure 3.1. Molecular structure and pK _a value for DA, CAT and DOPAC.	27

Figure 3.2. Cyclic voltammetric i-E curves for (A) microcrystalline diamond, (B) nanocrystalline diamond, and (C) GC electrodes in 0.1 M phosphate buffer, pH 2 (---) and pH 7 (—). Scan rate = 100 mV/s. Electrode geometric area = 0.16 cm². 28

Figure 3.3. Background current measured at 0 mV vs. pH for microcrystalline diamond (◆), nanocrystalline diamond (■), and glassy carbon (▲) electrodes in 0.1 M phosphate buffer. Scan rate = 100 mV/s. Electrode geometric area = 0.16 cm². Each data point and error bar represent the average and standard deviation of three measurements. 29

Figure 3.4. Cyclic voltammetric i-E curves for GC in 0.1 M phosphate buffer, pH 2, 4, and 7. Scan rate = 100 mV/s. Electrode geometric area = 0.16 cm². 31

Figure 3.5. Cyclic voltammetric i-E curves (background-subtracted) for microcrystalline diamond (—) and GC (—) electrodes in 10 μM DA, CAT, and DOPAC in 0.1 M phosphate buffer, pH 7. Scan rate = 100 mV/s. Electrode geometric area = 0.16 cm². 33

Figure 3.6. Cyclic voltammetric i-E curves (background-subtracted) for microcrystalline diamond (—) and GC (—) electrodes in 10 μM DA, CAT, and DOPAC in 0.1 M phosphate buffer, pH 2. Scan rate = 100 mV/s. Electrode geometric area = 0.16 cm². 34

Figure 3.7. Dopamine (A) oxidizes to duroquinone (B). The 6-position is susceptible to nucleophilic attack by the side-chain amine forming 5,6-dihydroxyindoline (C). 35

Figure 3.8. Plots of oxidation peak current vs. pH for microcrystalline diamond (◆), nanocrystalline diamond (■), and GC (▲) electrodes in 10 μM DA, CAT, and DOPAC in 0.1 M phosphate buffer. Scan rate = 100 mV/s. Electrode geometric area = 0.16 cm². The theoretical *i_p* value is indicated by the dashed line. 37

Figure 3.9. Plots of oxidation peak potential vs. pH for (A) microcrystalline diamond, (B) nanocrystalline diamond, and (C) GC electrodes in 10 μM solutions of DA (■), CAT (◆), and DOPAC (▲) in 0.1 M phosphate buffer. Scan rate = 100 mV/s. Electrode geometric area = 0.16 cm². 39

Figure 3.10. Surface functional groups on oxidized sp^2 and sp^3 electrodes.	42
Figure 3.11. The solution flow in a thin-layer electrochemical flow cell.	45
Figure 3.12. FIA-EC hydrodynamic voltammetric background i-E curves for microcrystalline diamond (◆), nanocrystalline diamond (■), and GC (▲) electrodes in 0.1 M phosphate buffer, 0.1 M NaCl, pH 7.2. Flow rate = 1.0 mL/min. Electrode geometric area = 0.12 cm ²	46
Figure 3.13. Peak-to-peak noise at microcrystalline diamond (■), nanocrystalline diamond (⊞), and GC (□) electrodes in 0.1 M phosphate buffer, 0.1 M NaCl, pH 7.2, as a function of applied potential. Flow rate = 1.0 mL/min. Electrode geometric area = 0.12 cm ²	48
Figure 3.14. Hydrodynamic voltammetric i-E curves for 20 μL injections of 30 μM catechols and catecholamines in microcrystalline diamond (◆), nanocrystalline diamond (■), and GC (▲). The carrier solution was 0.1 M phosphate buffer, 0.1 M NaCl, pH 7.2. Flow rate = 1.0 mL/min. Electrode geometric area = 0.12 cm ²	50
Figure 3.15. Calibration curves for the catechols and catecholamines obtained at (A) microcrystalline diamond, (B) nanocrystalline diamond, and (C) GC electrodes. Note: At least 5 concentrations were used for each curve but some plots appear to have fewer points because more measurements were made at the low μM level. The carrier solution was 0.1 M phosphate buffer, 0.1 M NaCl, pH 7.2. Flow rate = 1.0 mL/min. Injected volume = 20 μL. Electrode geometric area = 0.12 cm ²	55
Figure 3.16. FIA-EC response for 20-μL injections of 2 mM NE at microcrystalline diamond (◆), nanocrystalline diamond (■), and GC (▲) recorded over a 7-h period. The carrier solution was a Krebs's buffer, pH 7.4, flowing at 1.0 mL/min. Electrode geometric area = 0.12 cm ² . Each data point shown represents an average of 10 injections made at 1.0 min intervals.	57

Figure 3.17. FIA-EC response for 20- μ L injections of 1 μ M NE (injections 1-10) and 1 μ M NE with 1 mM BSA (injections 11-20) at microcrystalline diamond (\blacklozenge), nanocrystalline diamond (\blacksquare), and GC (\blacktriangle) electrodes. The carrier solution was a Kreb's buffer, pH 7.4, flowing at 1.0 mL/min. Injections were made at 1.0 min intervals. Electrode geometric area = 0.12 cm². 59

Figure 4.1. Steps in the metabolism of catecholamines. 63

Figure 4.2. Reversed-phase HPLC separation of 20 μ M DOPEG, NE, EP, VMA, NMN and MN on a C₁₈ column (Alltech Adsorbosphere HS, 5 μ m particle size, 4.6 mm x 150 mm). The mobile phase was 95/5 (v/v) 0.05 M NaH₂PO₄/MeOH, pH 2.5, 0.475 mM HSA. The working electrode was a nanocrystalline diamond thin film and the detection potential was 950 mV vs. Ag/AgCl. Flow rate = 0.8 mL/min. Injection volume = 20 μ L. Electrode geometric area = 0.12 cm². 66

Figure 4.3. Calibration curves obtained at a (A) nanocrystalline and (B) microcrystalline diamond thin-film electrode for a series of mixtures of the catecholamines and metabolites. The separation was carried out using the same conditions as in Figure 4.2. The detection potentials used were 950 mV and 1000 mV vs. Ag/AgCl for A and B, respectively. Injection volume = 20 μ L. Electrode geometric area = 0.12 cm². 68

Figure 4.4. Reversed-phase chromatograms for the analysis of plasma samples from (A) a normotensive rat and (B) a hypertensive rat on a C₁₈ column (Alltech Adsorbosphere HS, 5 μ m particle size, 4.6 mm x 150 mm). The mobile phase was 96/4 (v/v) 0.05 M NaH₂PO₄/MeOH, pH 2.5, 0.48 mM HSA. The working electrode was a nanocrystalline diamond thin film and the detection potential was 950 mV vs. Ag/AgCl. Flow rate = 0.8 mL/min. Injection volume = 20 μ L. Electrode geometric area = 0.12 cm². 71

Chapter 1

INTRODUCTION

Catechols are aromatic compounds with a single benzene ring structure and two substituent hydroxy groups at 3- and 4- positions, and are widely distributed in living systems. For example, they comprise the toxic substance found in poison ivy that causes allergic contact dermatitis.¹ Catecholamines, substituted catechols with an amino group in a side chain, function as neurotransmitters in the central nervous system. They play a vital role in human disorders, such as depression and schizophrenia. They are involved in a variety of regulatory systems, such as emotion, stress, learning and sleep. They also take part in many metabolic processes like hormone secretion.²

Abnormal levels of catecholamines and their metabolites in biological fluids can be used for the diagnosis of certain diseases. For example, patients with pheochromocytoma, a tumor of chromaffin cells in the adrenal gland, have elevated levels of norepinephrine and epinephrine in urine.³ Abnormal catecholamine content in the heart, a principal location of catecholamine synthesis and storage, is associated with cardiovascular disease. Congestive heart failure has been linked to reduced myocardial norepinephrine and elevated urinary norepinephrine. Catecholamine levels in plasma have been used to diagnose hypertension.⁴

The development of techniques for the quantification of catechols and catecholamines is essential due to the wide range of functions these molecules serve. The

catecholamine content in urine, plasma, and cerebrospinal fluid is of clinical interest as it can serve as a marker for a variety of metabolic, cardiovascular, and neurological abnormalities.⁵ Several methods have been used to measure catecholamines including absorbance and fluorescence detection, radioenzymatic methods, mass spectrometry and electrochemical (EC) detection. One advantage of EC detection over other analytical methods for catecholamine measurement is that there is no need for a derivatization procedure prior to analysis. EC detection is also noted for its superior sensitivity compared to other methods. Table 1.1 presents the detection limits obtained for the catecholamines, norepinephrine, epinephrine and dopamine, using ultraviolet, fluorescence and EC detection coupled with liquid chromatographic separation under optimal experimental conditions.⁶ Other benefits include good precision, simple instrumentation, and low cost.

Table 1.1. Detection limits for the catecholamines with ultraviolet, fluorescence and EC detection.⁶

	Ultraviolet	Fluorescence	Electrochemical
Norepinephrine	5 ng	2 ng	0.015 ng
Epinephrine	5 ng	2 ng	0.15 ng
Dopamine	5 ng	5 ng	0.20 ng

Many catechols and catecholamines are electrochemically-active and are thus ideally suited for EC detection. They can be readily oxidized to generate the corresponding orthoquinone via a two-proton, two-electron reversible redox reaction, as shown in Figure 1.1

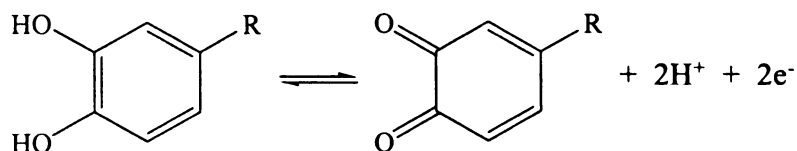


Figure 1.1. The catechol/orthoquinone redox reaction.

In an electrochemical measurement, the potential applied to a working electrode with respect to a reference electrode serves as the driving force for the redox reaction. The working electrode then acts as an electron sink or source, depending on the magnitude of the applied potential. Measurement of the current that flows in response to the applied potential can be used to determine the redox analyte concentration in solution.⁷

A limitation with electroanalytical measurements is that the molecular specificity is often lacking due to the fact that different analytes undergo electrolysis at similar potentials. For example, many of the catechols and catecholamines can undergo electron transfer at similar potentials, making it difficult to extract qualitative information from a measurement of a solution containing multiple analytes.^{7,8} In many cases, a separation step such as reversed-phase liquid chromatography or capillary electrophoresis is coupled to EC detection.^{2,3} High performance liquid chromatography with electrochemical detection (HPLC-EC) still remains one of the most widely used methods for catecholamine and related compound analysis since the technique was introduced in the 1970s.^{9,10} It is the method of choice in most clinical laboratories and physiological research for its high selectivity, good reproducibility, simple instrumentation, short analysis time, and low cost.

Another main shortcoming of EC detection is the deactivation that is often observed with electrodes during use. Deactivation refers to attenuated current and decreased electrode reaction kinetics. Carbon electrodes, in particular, are subject to a gradual loss of activity due to changes in the electrode microstructure and chemistry and electrode fouling by adsorbed reaction intermediates and products.¹¹ The presence of electroactive and ionizable surface carbon-oxygen functionalities on the commonly used sp^2 carbon electrodes, as illustrated in Figure 1.2, present additional complications.¹² These include increased background current, pH-dependence of background and faradaic signals, susceptibility to fouling due to strong molecular adsorption, need for frequent pretreatment, large response variability, and poor response precision.¹²

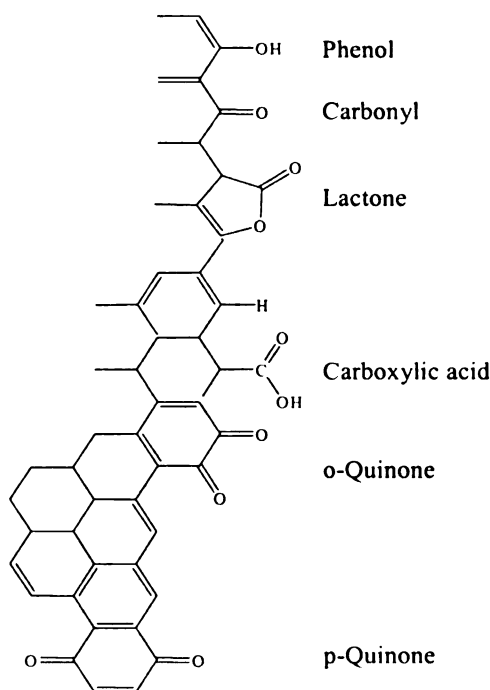


Figure 1.2. Representative functional groups that might exist on oxidized sp^2 carbon surfaces.

Given the above mentioned issues with sp^2 carbon materials, it would be advantageous to have an electrode that is devoid of surface carbon-oxygen functionalities but is still responsive to the analytes of interest. A promising new, oxygen-free electrode material is electrically conducting, boron-doped diamond. The atomic structure of diamond, as shown in Figure 1.3, consists of an extended network of sp^3 -bonded carbon atoms in a tetrahedral arrangement. The surface carbon atoms are stabilized by strong covalent bonds with hydrogen for films deposited from hydrogen-rich source gas mixtures. Diamond is the stable form of carbon at high pressure and temperature.¹³ It is a unique material with exceptional properties like extreme hardness, high thermal conductivity, high chemical inertness, and low compressibility. Diamond is sometimes referred to as the “ultimate engineering material” because of its exceptional properties. There is interest in using diamond in a variety of applications, such as optics, electronics, and thermal management.^{13,14} One application that has gained prominence in recent years is conductive diamond electrodes for electrochemistry.

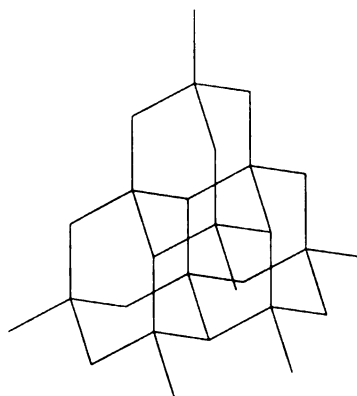


Figure 1.3. The cubic diamond crystal lattice.

The first reports of diamond electrodes for electrochemistry were in the mid-1980s.^{15,16} Although diamond is a very good electrical insulator, it can possess semimetal electronic properties when doped with boron and thus be utilized in electrochemical measurements. In boron-doped, thin-film diamond electrodes, boron atoms substitute in place of carbon atoms during film growth.^{17,18} Boron functions as an electron acceptor and promotes *p*-type semiconductivity with an acceptor activation energy of 0.37 eV above the valence band. Valence band electrons are thermally promoted to the boron acceptors, leaving free electrons in the dopant band, and holes in the valence band to support current flow. Electrical conductivity is influenced not only by the boron-doping level, but also by the grain boundaries at the surface and the nondiamond sp^2 carbon impurity that might be present.¹⁷

High quality, hydrogen-terminated diamond possesses several interesting and electroanalytically important properties that distinguish it from other sp^2 carbon electrodes. Untreated diamond films exhibit good electrochemical activity for a number of redox systems without conventional pretreatment. One remarkable property is its chemical stability in harsh or corrosive environments. Due to weak molecular adsorption, the hydrogen-terminated electrode resists deactivation during long-term exposure to air or electrolyte solutions. Conventional sp^2 carbon electrodes, on the other hand, often deactivate quickly during exposure to electrolyte solution or to air.¹⁸ For this reason, frequent pretreatment such as polishing must be performed and utmost care must be taken in order to achieve a clean surface with reproducible properties.

Diamond thin films exhibit a large working potential window in aqueous media. The material exhibits large overpotentials for oxygen and hydrogen evolution presumably because there are few low energy sites available for the adsorbed reaction intermediates.¹⁹⁻²¹ Figure 1.4 shows a cyclic voltammetric i-E curve for a diamond thin film in 1.0 M KCl. The working potential window, defined as the potential range between the points at which anodic and cathodic currents reach $\pm 50 \mu\text{A}$, is about 3.5 V. The wide working potential window permits the electrochemistry of redox couples with large positive or negative standard reduction potentials to be studied, something that would otherwise be impossible due to interference from solvent electrolysis. Diamond also exhibits a low and featureless background current. This results in enhanced signal-to-background (S/B) ratios in electroanalytical measurements.¹⁷

Hydrogen-terminated diamond electrodes, in contrast with oxygen-containing sp^2 carbon electrodes, are relatively inert to the adsorption of polar molecules as shown by experiments conducted on the adsorption of anthraquinone-2,6-disulfonate (AQDS) to glassy carbon, graphite and diamond electrodes.²² Physisorption of AQDS was not observed on diamond presumably because of the relative absence of polar carbon-oxygen functional groups which promote strong dipole-dipole and ion-dipole interactions with the adsorbate. Diamond electrodes are thus quite useful for electroanalytical measurements in which the analyte of interest exists in a complex mixture containing contaminants that tend to adsorb and foul conventional carbon electrodes.¹⁷

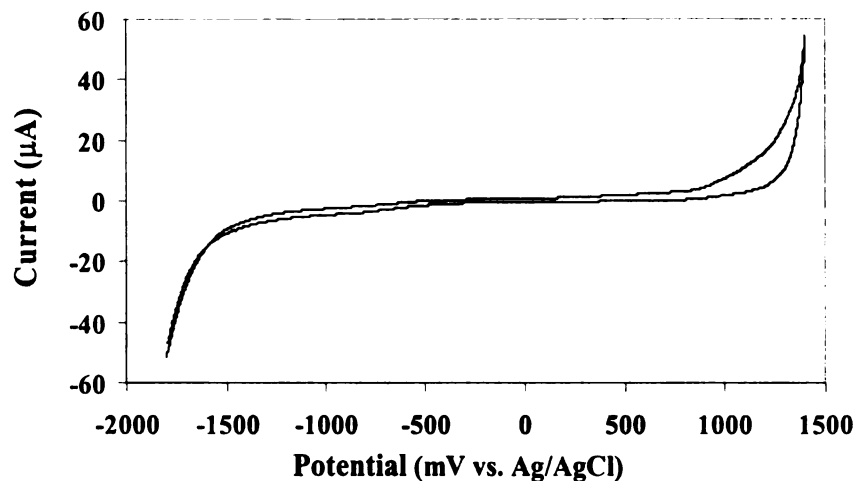


Figure 1.4. Background cyclic voltammetric i-E curves in 1.0 M KCl for a microcrystalline diamond film. Scan rate = 100 mV/s. Electrode geometric area = 0.16 cm².

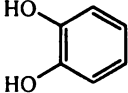
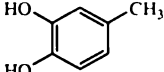
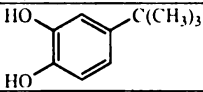
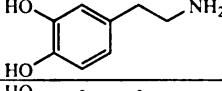
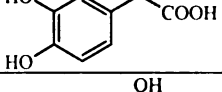
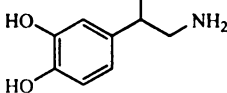
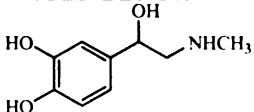
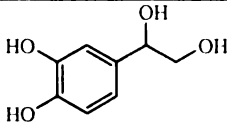
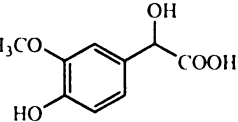
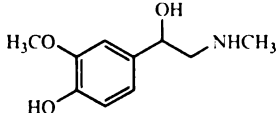
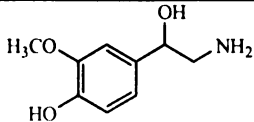
Polycrystalline diamond thin-film electrodes have been shown to outperform glassy carbon, a conventional sp² carbon electrode, for the electrochemical detection of azide,^{23,24} trace levels of metal ions,²³ chlorpromazine,²³ aliphatic polyamines,²⁵⁻²⁷ and chlorinated phenols²⁸ using flow injection analysis. The detection of carbamate pesticides,²⁹ NADH,³⁰ uric acid,³¹ and histamine and serotonin³² has also been reported. Untreated diamond was shown to have a slightly lower sensitivity for 4-methyl catechol and dopamine as compared to freshly polished glassy carbon, but the detection limit and response precision are superior due to lower background current and noise for the former.²³ Diamond microelectrodes have been used for the electrochemical detection of catechol and dopamine in capillary electrophoresis, and exhibited low background current and noise, good response precision, wide linear dynamic range, and limits of

detection at fmol level.³³ The modification of diamond microfiber electrodes with overoxidized polypyrrole (OPPy) has been shown to enhance the response selectivity, sensitivity and stability for the amperometric detection of dopamine in the presence of *in vivo* interfering compounds, such as ascorbic acid and 3,4-dihydroxyphenylacetic acid.³⁴

The goals of the research described herein were (i) to study the electrochemical behavior of various catecholamines and metabolites at microcrystalline and nanocrystalline diamond electrodes as a function of the solution pH, and (ii) to evaluate the performance of both diamond electrode types for the amperometric detection of these analytes when coupled with HPLC. This research was motivated by our desire to better understand how the surface microstructure and chemistry of diamond electrodes affect the electrochemical response for these compounds and to improve the detection figures of merit in HPLC, as compared to what can be achieved with commonly used sp^2 carbon electrodes. A table of the molecular structure and pK_a of the analytes used in this research is presented in Table 1.2.³⁵

Cyclic voltammetry was used to investigate the electrochemical behavior of various catechols and catecholamines at two diamond types - microcrystalline and nanocrystalline diamond thin films. Comparison measurements were made with glassy carbon. One main issue addressed was whether or not the redox chemistry of these analytes proceeds through an adsorbed state as in the case for sp^2 carbon electrodes. Another issue studied was the pH-dependence of the background current and the voltammetric response of the analytes at the hydrogen-terminated diamond electrode.

Table 1.2. Molecular structure, pK_a ³⁵ and formula mass of the analytes.

Analyte	Molecular structure	pK_a values	Formula Mass (g/mol)
catechol (CAT)		9.50	110.11
4-methyl catechol (MC)		9.69	124.14
4-t-butyl catechol (BC)		9.66	166.22
dopamine (DA)		9.41, 9.99	153.18
3,4-dihydroxyphenylacetic acid (DOPAC)		4.42	168.15
norepinephrine (NE)		9.57, 8.30	169.18
epinephrine (EP)		9.60, 9.16	183.20
3,4-dihydroxyphenylglycol (DOPEG)		9.55	170.16
vanillylmandelic acid (VMA)		3.42	198.17
metanephrine (MN)		9.78, 9.13	197.23
normetanephrine (NMN)		9.76, 8.25	183.20

Amperometric detection using both diamond types was employed with flow injection analysis and reversed-phase liquid chromatography to assay for the analytes. The electrochemical performance of diamond was compared with that of glassy carbon. The goal was to determine if diamond electrodes provide significantly improved detection figures of merit (e.g., linear dynamic range, sensitivity, limit of detection, response precision and response stability) for the catecholamines and metabolites as compared to glassy carbon. The bioanalytical applicability of the assay was demonstrated in a preliminary way using plasma samples from normotensive and hypertensive rats. The work was our initial effort at applying HPLC-EC with diamond electrodes for monitoring catecholamine levels in biological fluids.

Chapter 2

EXPERIMENTAL METHODS

2.1. Boron-Doped Diamond Thin-Film Growth

The procedure for diamond film growth has been described elsewhere.^{23,36} The diamond thin films were deposited on p-type Si(100) substrates ($\sim 10^{-3}$ Ω -cm, Virginia Semiconductor Inc.) using a commercial microwave-assisted chemical vapor deposition (CVD) system (1.5 kW, Astex, Inc.). The substrate surface was mechanically scratched on a felt polishing pad with 1 μ m diameter diamond powder (GE Superabrasives). The scratched substrate was then extensively washed with ultrapure water, isopropyl alcohol (IPA), acetone, IPA, and ultrapure water to remove the polishing debris. During the scratching process, some of the diamond particles are embedded into the surface. Both the clean polishing striations and the embedded diamond particles serve as nucleation sites for film growth. The cleaned substrate was then placed in the CVD reactor.

The microcrystalline diamond films were grown using a methane (CH_4) / hydrogen (H_2) volumetric ratio of 0.50% at a total flow of 200 sccm, a microwave power of 1000 W, a growth pressure of 45 torr, an estimated substrate temperature of 800 $^\circ\text{C}$, and a growth time of 10 h. Ultrahigh purity (99.999%) CH_4 and H_2 were used as the source gases. Diborane (B_2H_6) diluted in hydrogen (0.1%) was used for boron doping. The concentration of B_2H_6 added to the source gas was 1 ppm. The plasma was ignited with all gases flowing to initiate the deposition. After growth, the CH_4 and B_2H_6 flows were

stopped and the films remained exposed to the H₂ plasma for an additional 10 min. After this period, the microwave power and system pressure was gradually reduced down to 400 W and 10 mtorr over a 15-min period to cool the samples in the presence of atomic hydrogen. Post-growth treatment in atomic hydrogen is essential for removing adventitious non-diamond carbon impurity and ensuring full hydrogen surface termination. The film thickness was 4 - 6 μm and the resistivity was 0.01 Ω-cm, or less.

The nanocrystalline diamond films were synthesized using ultrahigh purity CH₄, Ar, and H₂ (99.999%) at flow rates of 1, 94, and 5 sccm, respectively. B₂H₆, diluted in hydrogen (0.1%), was used for boron doping. The concentration added to the source gas was 1 ppm. The microwave power and deposition pressure were maintained at 800 W and 140 torr, respectively. The substrate temperature was estimated by optical pyrometry to be about 800 °C. The deposition time was 2 h. The plasma was ignited with all gases flowing to initiate the deposition. At the end of the deposition period, the CH₄ and B₂H₆ flows were stopped and the Ar and H₂ flows continued. The film was then exposed to an H₂/Ar plasma for 10 min. The substrate was then cooled in the presence of atomic hydrogen to an estimated temperature of less than 400 °C by slowly reducing the power and pressure over a 4-min period. The resulting diamond films were approximately 4 - 7 μm thick with a resistivity of 0.3 Ω-cm, or less.

2.2. Boron-Doped Diamond Thin-Film Characterization

2.2.1. Atomic Force Microscopy

Atomic force microscopy (AFM) was used to examine the diamond film morphology.²³ The measurements were performed using a Nanoscope III instrument

(Digital Instruments) in the contact mode. Si_3N_4 probe tips, mounted on Au cantilevers (100 μm) with spring constants ranging from 0.54 to 0.06 N/m, were used to acquire topographical images of the films in air.

Typical AFM images of a (A) microcrystalline and (B) nanocrystalline diamond film are presented in Figure 2.1. These images show that the nanocrystalline film has smoother surface, smaller grain size, and greater fraction of grain boundary compared to the microcrystalline film. Microcrystalline films are well-faceted with a predominance of octahedral and cubo-octahedral crystallites. The nominal crystallite size is in the range of 1 to 3 μm .²⁸ Nanocrystalline films consist of nodular features of $\sim 50 - 100$ nm in diameter. These features are actually aggregates of ~ 15 nm diameter grains of diamond that form as a result of the high rate of nucleation.³⁶

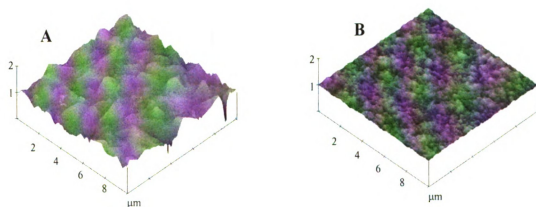


Figure 2.1. AFM images (contact mode, air) of a (A) microcrystalline and (B) nanocrystalline diamond thin film.

2.2.2. X-ray Diffraction

X-ray diffraction (XRD) was employed to characterize the bulk crystallinity of the diamond thin films.³⁶ A Rigaku Rotaflex diffractometer equipped with a rotating

anode and a Cu K-alpha radiation source was used to obtain the XRD patterns. The thin film rotates by an angle, θ , with respect to a fixed x-ray source, and the detector rotates by 2θ to measure the reflected light. The measurements were made from 2θ of 30° to 100° .

Figure 2.2 shows the XRD spectra for a (A) microcrystalline and (B) nanocrystalline diamond thin film. For both films, three reflections are observed at 2θ values of 44° , 76° , and 92° , and are assigned to the (111), (220), and (311) planes of cubic diamond, respectively.³⁶ The peaks for the nanocrystalline film are broader than those for the microcrystalline film due to the smaller grain size. This result confirms that both film types possess a crystalline diamond structure.

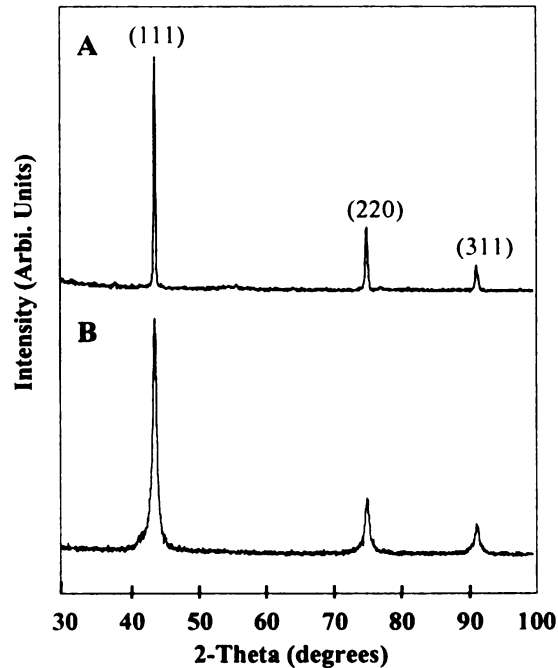


Figure 2.2. XRD pattern for a (A) microcrystalline and (B) nanocrystalline diamond thin film.

2.2.3. Raman Spectroscopy

Raman spectroscopy was used to evaluate the film microstructure and to detect the presence of nondiamond sp^2 -bonded carbon impurity.³⁶ Raman spectra were obtained with a Raman 2000 spectrometer equipped with a microprobe attachment (2080) and a direct video module (2090) (Chromex, Inc.) in a 180° back-scattered collection mode. The spectra were obtained using a 1200 groove/mm holographic grating. Excitation was from a frequency-doubled Nd:YAG (532 nm, 30 mW) laser. The laser beam was focused to a spot size of approximately 5 μm resulting in an estimated power density of 150 kW/cm^2 . Spectra were collected with a 10 s acquisition time. The spectrometer was calibrated with a piece of single crystal (Type IIa) diamond standard (100 orientation, Harris diamond) prior to use.

Figure 2.3 shows Raman spectra for microcrystalline and nanocrystalline diamond. A sharp peak at 1332 cm^{-1} is seen for the microcrystalline film and is characteristic of high quality diamond originating from the sp^3 -bonded carbon structure. It is the first-order phonon for diamond. For nanocrystalline diamond, this peak has a broader peak width and sits atop a large background signal. There are two possible explanations for the line broadening. The first is the surface confinement model which states that the smaller the domain size, the larger the range of phonon modes that are allowed to participate in the Raman process. The broad line width is due to the spread in phonon energy. Another explanation is phonon scattering by impurities and defects (i.e., grain boundaries). The scattering shortens the phonon lifetime resulting to the broadening of the Raman line.³⁷ Birrell et al. recently proposed that the origin of this peak is sp^2 -bonded carbon in the grain boundary and not sp^3 -bonded carbon.³⁸ The peak at 1150

cm^{-1} is a signature for high quality nanocrystalline diamond, but its origin has not yet been confirmed. Ferrari and Robertson assigned this peak to sp^2 -bonded carbon transpolyacetylene segments at grain boundaries.³⁹ The 1550 cm^{-1} peak is assigned to disordered sp^2 carbon in the grain boundaries. It is downshifted from the expected 1580 cm^{-1} position as in graphite because the sp^2 -bonded carbon is amorphous and is mixed with sp^3 -bonded carbon. In the nanocrystalline film, the sp^2 -bonded carbon is confined to the abrupt grain boundaries which consist of a network of 3- and 4-fold coordinated carbon atoms.⁴⁰

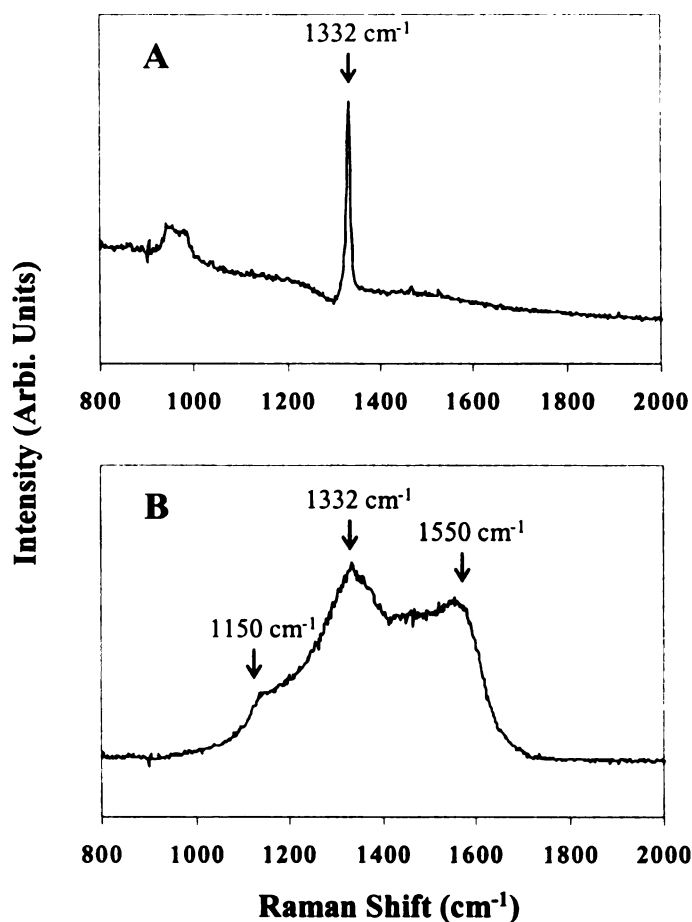


Figure 2.3. Visible Raman spectra for a (A) microcrystalline and (B) nanocrystalline diamond thin film. $\lambda_{\text{ex}} = 532 \text{ nm}$. Laser power = 30 mW. Integration time = 10 s.

2.2.4. Contact Angle Measurement

The contact angle for water was measured to determine the relative hydrophobicity of the diamond thin-film surface. A hydrogen-terminated surface is more hydrophobic than an oxygen-terminated one and should exhibit a larger contact angle for clean water. For example, Ostrovskaya and coworkers found that hydrogenation of CVD diamond films in an H₂ plasma increases the hydrophobic nature of the surface, as the contact angle for water increases from $\theta = 32^\circ$ for an oxidized surface to up to $\theta = 93^\circ$ after hydrogenation.⁴¹

An automated contact angle apparatus (First Ten Angstroms) was used to deliver a 10 μ L drop of deionized water from a 50-mL syringe on to the diamond surface. The drop was formed at the end of the blunt, stainless steel syringe needle and the diamond film was then raised slowly to touch the drop. Images of the static drop on the film surface were captured with a video camera. The contact angle was obtained using image analysis software which fitted a curve to the drop image and calculated the line tangent to the curve. The angle between the tangent line and the electrode surface was measured at the left and right sides of the drop. The right and left angles were averaged to give one contact angle value. Five measurements were made on a single film, with the electrode rinsed with acetone and dried under N₂ between measurements. Four microcrystalline diamond thin-film electrodes were tested and gave contact angles of $69.2 \pm 5.5^\circ$, $64.0 \pm 3.0^\circ$, $72.8 \pm 2.3^\circ$, and $75.3 \pm 5.1^\circ$.

2.2.5. Cyclic Voltammetry

Electrochemical characterization of the films was carried out by cyclic voltammetry (CV) using $\text{Fe}(\text{CN})_6^{3-/4-}$ and $\text{Ru}(\text{NH}_3)_6^{3+/2+}$ as redox test systems. The physical, chemical and electronic properties of a diamond thin-film electrode influence the electrode reaction kinetics and mechanisms for these systems.

Solutions of 1.0 mM potassium ferrocyanide ($\text{K}_4\text{Fe}(\text{CN})_6$, Aldrich) and 1.0 mM hexaamine ruthenium(III) chloride ($\text{Ru}(\text{NH}_3)_6\text{Cl}$, Aldrich) were freshly prepared in 1.0 M potassium chloride (KCl, Fisher) solution. CV was performed with a CS-1090 digital potentiostat (Cypress Systems) using a single compartment, three-electrode glass cell. The cell design is shown in Figure 2.4.

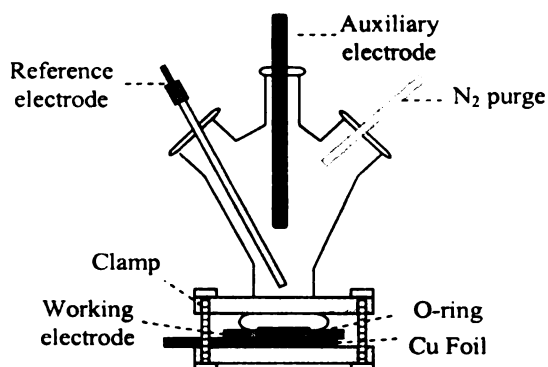


Figure 2.4. Diagram of the single compartment, glass electrochemical cell.

The planar working electrode was pressed against a smooth glass joint at the bottom of the cell. A VitonTM o-ring was used to define the geometric area exposed to the solution. A large-area carbon rod served as the auxiliary electrode and an Ag/AgCl electrode (3 M NaCl, Cypress Systems) was used as the reference. All potentials are reported versus this reference.

Typical CV curves for the two redox analytes are shown in Figure 2.5. A summary of the CV data is presented in Table 2.1. The CV data noted are the oxidation and reduction

peak potentials (E_p^{ox} and E_p^{red}) and the oxidation and reduction peak currents (i_p^{ox} and i_p^{red}). Of particular importance is the peak potential separation ($\Delta E_p = E_p^{\text{ox}} - E_p^{\text{red}}$), which reflects the rate of the redox reaction. The electrode kinetics for $\text{Fe}(\text{CN})_6^{3-/4-}$ system are strongly influenced by the physicochemical properties of diamond. ΔE_p is very sensitive to the surface chemistry with the lowest values seen for clean surfaces with low oxide coverage. Surface oxygen apparently blocks a surface site that is involved in the reaction on the hydrogen-terminated surface.⁴² The kinetics of the $\text{Ru}(\text{NH}_3)_6^{3+/2+}$ system are much less sensitive to the physicochemical properties of both sp^2 carbon and diamond electrodes. ΔE_p , for example, is insensitive of surface modification indicating that electron transfer step does not involve an interaction with a surface site or functional group.⁴³ ΔE_p is most influenced by the electronic properties of the electrode particularly the density of electronic states near the formal potential of the redox system. ΔE_p increases as the boron doping level of the diamond electrode decreases.⁴⁴

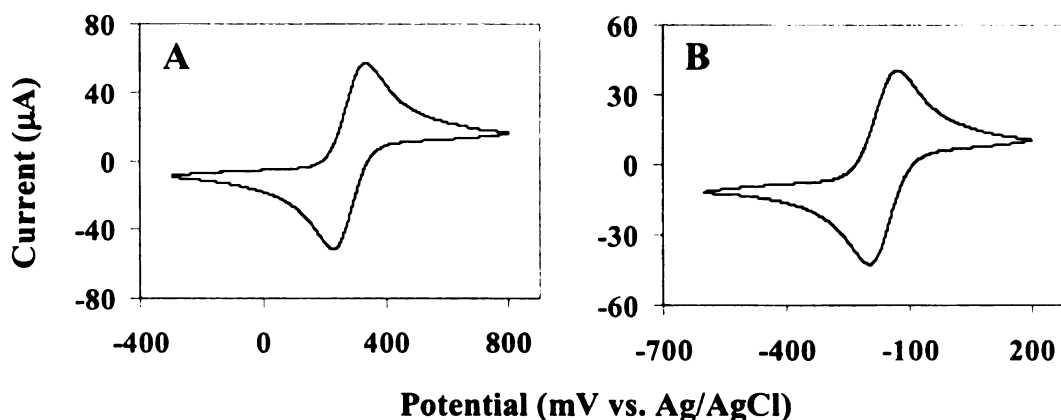


Figure 2.5. Cyclic voltammetric i-E curves for (A) 1.0 mM $\text{Fe}(\text{CN})_6^{3-/4-}$ and (B) 1.0 mM $\text{Ru}(\text{NH}_3)_6^{3+/2+}$ at a microcrystalline diamond thin film. The supporting electrolyte was 1.0 M KCl. Scan rate = 100 mV/s. Electrode geometric area = 0.16 cm².

Table 2.1. Cyclic voltammetric data for the redox test systems at a microcrystalline diamond thin-film electrode.

Analyte	ΔE_p (mV)	E_p^{ox} (mV)	i_p^{ox} (μA)	i_p^{ox}/i_p^{red}
1 mM $Fe(CN)_6^{3-/4-}$ /1 M KCl	91	323	62.2	1.00
1 mM $Ru(NH_3)_6^{3+/2+}$ /1 M KCl	66	-131	45.8	1.02

Note: Experimental conditions as described in Figure 2.5.

2.3. Glassy Carbon Polishing Procedure

The glassy carbon electrode (GC-30, Tokai) was polished with alumina powder (Buehler) slurred in ultrapure water ($\sim 18 M\Omega\text{-cm}$, Barnstead E-Pure) on a felt polishing cloth (Buehler). Alumina of decreasing grit size was used: 1.0, 0.3 and 0.05 μm . The electrode was sonicated in ultrapure water for 10 min after each polishing step. At the end of the polishing sequence, the electrode was thoroughly rinsed with water and allowed to soak in distilled IPA for 10 min prior to use. The electrode was used in electrochemical measurements immediately after polishing.

2.4. Flow Injection Analysis

Flow injection analysis (FIA) was performed using a home-made thin-layer electrochemical flow cell with a cross-flow geometry. The experimental set-up has been described elsewhere.²⁵ A block diagram of the FIA system and a schematic of the thin-layer electrochemical flow cell are shown in Figures 2.6 and 2.7.

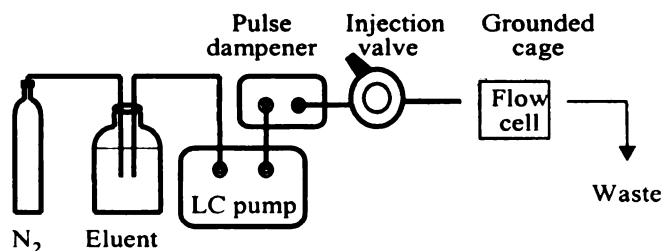


Figure 2.6. Block diagram of the FIA system.

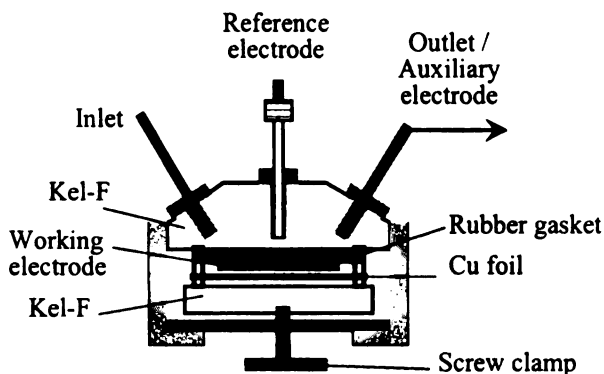


Figure 2.7. Schematic of the thin-layer flow cell.

The flow rate of the carrier solution was regulated with a consta-Metric III metering pump (Milton Roy), through a model 7125 injector valve (Rheodyne) with a 20- μ L injection loop, and into the flow cell. The carrier solution, flowing at 1.0 mL/min, was constantly sparged with nitrogen. Pump noise was reduced with a Model LP-21 pulse dampener (Scientific Systems). Amperometric detection was used and the current was recorded in analog form using a strip chart recorder. The entire set-up was grounded and the flow cell was housed in a Faraday cage to reduce the pick-up of electrical noise. The flow cell was constructed with two pieces of Kel-F. The top piece contained the inlet and outlet for the fluid flow and a place for the reference electrode. The outlet port was fitted with a short piece of stainless steel tubing that served as the counter electrode. The bottom piece supported the working electrode. Electrical contact was made by pressing a piece of copper foil against the back side of the planar working electrode. A

rubber gasket separated the surface of the working electrode from the top piece of the cell. A rectangular groove (0.80 cm x 0.15 cm x 0.10 cm) was cut into the gasket and this defined the flow channel. Assuming a 25% compression of the gasket when the top and bottom pieces of the cell were clamped together, the cell volume was estimated to be ~9 μL . An Omni-90 analog potentiostat (Cypress Systems) was employed to control the potential applied to the working electrode and to measure the current during amperometric detection. The potential was applied with respect to a commercial Ag/AgCl mini-electrode (3 M NaCl, Cypress Systems).

2.5. High Performance Liquid Chromatography

Reversed-phase high performance liquid chromatography (HPLC) was performed using a commercial system (Shimadzu Corp.) which consisted of a controller (SCL-10AVP), a solvent delivery module (LC-10ADVP), a degasser (DGU-14A), and an auto-injector (SIL-10ADVP). The mobile phase flow rate was maintained at 0.8 mL/min. The samples (20 μL) were injected onto a 5 μm , 4.6 mm x 150 mm Alltech Adsorbosphere HS C₁₈ column. The same thin-layer flow cell described above was used for electrochemical detection. An Omni-90 analog potentiostat (Cypress Systems Inc.) controlled the potential applied to the working electrode and measured the current during detection. Data were acquired in digital form with Class VP 7.0 software (Shimadzu).

2.6. Chemicals and Reagents

Reagent-grade quality chemicals and ultrapure distilled and deionized water (~18 M Ω -cm, Barnstead E-Pure) were used to prepare all solutions. Sodium phosphate

monobasic (monohydrate, NaH_2PO_4 , CCI), sodium phosphate dibasic (heptahydrate, Na_2HPO_4 , Spectrum), sodium chloride (NaCl , Spectrum), sodium hydroxide (NaOH , Spectrum), phosphoric acid (H_3PO_4 , 99.999+%, Aldrich), methanol (MeOH , HPLC grade, Spectrum) and 1-heptanesulfonic acid (sodium salt, 98%, Aldrich) were used to prepare the carrier solution/mobile phase for FIA and LC. For some FIA measurements, a Krebs's buffer was used as the carrier solution and was prepared as follows: 117 mM NaCl , 4.7 mM KCl , 2.5 mM calcium chloride (anhydrous, CaCl_2 Mallinckrodt), 1.2 mM magnesium chloride (MgCl_2 , 98%, Aldrich), 25 mM sodium bicarbonate (NaHCO_3 , Spectrum), 1.2 mM NaH_2PO_4 , and 11 mM glucose (anhydrous, Mallinckrodt). Bovine albumin (98%, Sigma) was used as an interfering biomolecule.

The catechol (99+%, Aldrich), 4-methyl catechol (95+%, Aldrich), 4-tert-butyl catechol (97%, Aldrich), dopamine (hydrochloride salt, Sigma), norepinephrine (L-bitartrate hydrate salt, 99%, Aldrich), epinephrine (99%, Aldrich), 3,4-dihydroxyphenyl acetic acid (Sigma), normetanephrine (hydrochloride salt, 98%, Sigma), metanephrine (DL-m-O-methylepinephrine hydrochloride, Sigma), vanillylmandelic acid (α ,4-dihydroxy-3-methoxybenzeneacetic acid, Sigma), DL-3,4-dihydroxyphenylglycol (Sigma) were used without any additional purification. Stock solutions were prepared monthly in 0.1 M perchloric acid (HClO_4 , 99.999%, Aldrich) and stored in the refrigerator. Dilution of the stock solution with the appropriate solvent to the desired concentration was done daily.

All glassware was cleaned by rinsing in a KOH /ethanol bath, then in an Alconox solution, and finally with ultrapure water.

Chapter 3

BORON-DOPED DIAMOND THIN-FILM ELECTRODES FOR THE ELECTROCHEMICAL DETECTION OF CATECHOLS AND CATECHOLAMINES

3.1. Cyclic Voltammetric Behavior of Catechols and Catecholamines

3.1.1. Introduction

Some molecules, such as catecholamines, that serve as messengers between biological cells, are easily oxidized and therefore can be electrochemically detected. Adams and coworkers pioneered the use of electrochemistry to monitor neurotransmitters in the 1970s.⁴⁵ Their motivations were to develop a sensitive catecholamine assay for use with brain tissue and cerebrospinal fluid, and to use carbon microelectrodes for the *in vivo* monitoring of catecholamines and metabolites. Over the years, electrochemical methods have been used extensively for neurochemical monitoring with much emphasis on enhancing the response sensitivity and selectivity.¹² Fast-scan cyclic voltammetry (CV) and chronoamperometry are two most widely used techniques.⁴⁶

CV is a powerful tool for generating kinetic and mechanistic information about an electroactive compound. The technique involves linearly scanning the potential applied to an electrode immersed in an unstirred solution, from an initial value to a final or switching value and then back to the initial value. A potentiostat controls the potential applied to the working electrode with respect to a reference electrode, and measures the current that flows between the working and counter electrodes. The resulting data is a

plot of current versus potential called a cyclic voltammogram.^{47, 48} CV is a very versatile technique that can be used to study the thermodynamics of redox processes, to evaluate the effects of various electrode surface conditions on a redox reaction's kinetics and mechanism, and to investigate coupled chemical reactions and adsorption processes. The technique can also be used to determine the redox potential of the electroactive species.⁴⁹

It can be difficult to use CV to analyze complex mixtures because of the limited selectivity the technique affords, especially when multiple analytes that undergo redox reaction at similar potentials are present. Despite this limitation, CV is routinely employed for the analysis of neurotransmitters and related compounds using microelectrodes at fast scan rates.⁵⁰ Carbon fiber is the most commonly used electrode type for these measurements. The technique offers good temporal resolution to follow the rapid concentration dynamics of the analyte.⁵⁰ Identification of a redox-active species is possible based on the shape of the cyclic voltammogram. It should be noted that the response time, selectivity, and sensitivity are critically dependent on the condition of the electrode surface.⁴⁶ The control of electrode surface properties has been investigated extensively in order to optimize the electrode performance for the electrochemical detection of catecholamines. For example, selectivity is enhanced by coating electrodes with Nafion, which acts as an electrostatic gate that preconcentrates cationic species (catecholamines) and repels anionic interferents (ascorbic acid).⁵¹ The effects of surface pretreatments such as electrochemical polarization, vacuum heat treatment, anaerobic polishing and chemisorption of molecular adlayers on the electrode reaction kinetics for catechols and catecholamines at glassy carbon (GC) has been studied thoroughly by McCreery and coworkers. Fast electron transfer has been correlated with enhanced

catechol adsorption on the electrode surface with a “self-catalysis” mechanism being proposed.⁵²

In this Chapter, cyclic voltammetric studies of the electrochemical behavior of dopamine (DA), catechol (CAT), and 3,4-dihydroxyphenylacetic acid (DOPAC) at microcrystalline and nanocrystalline diamond thin-film electrodes are discussed. The molecular structure and pK_a value³⁵ of each analyte are shown in Figure 3.1. These analytes were selected in order to probe the electrode response for a cationic, neutral, and anionic redox system at pH 7. The CV curves were used to assess whether or not adsorption is a part of the electrode reaction mechanism at the two diamond types. The behavior for GC is also presented for comparison. The pH-dependence of the electrochemical response was also studied with focus on understanding the order of H^+ and e^- transfer for the redox analytes and probing the effects of the electrode surface chemistry on the electrode response. Again, studies with GC are reported, for comparison.

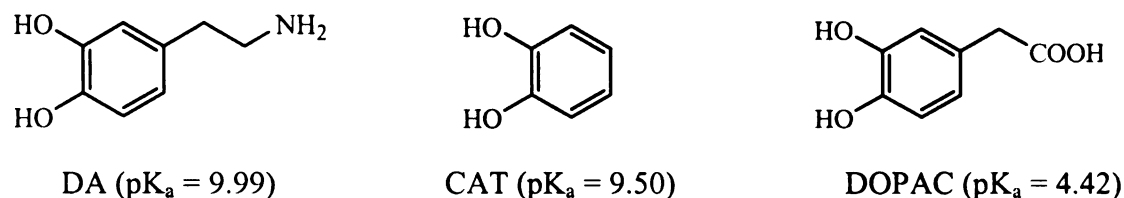


Figure 3.1. Molecular structure and pK_a value for DA, CAT and DOPAC.

3.1.2. Results and Discussion

Cyclic voltammetric background i - E curves were recorded for microcrystalline diamond, nanocrystalline diamond and freshly polished GC in 0.1 M phosphate buffer solutions (0.1 M NaH_2PO_4 + 0.1 M Na_2HPO_4) of pH 2, 3, 4, 5, 6, and 7. The electrode

geometric area was 0.16 cm^2 and the potential was scanned from -500 to $+500 \text{ mV}$ vs. Ag/AgCl at a scan rate (ν) of 100 mV/s . Three measurements were made with each electrode type. A different electrode was used for each measurement in the case of the microcrystalline and nanocrystalline diamond films, while only one piece of GC was used that was mechanically polished between measurements. The diamond films were used as is without any activation pretreatment. Representative cyclic voltammograms at pH 2 and 7 are shown in Figure 3.2. The anodic background current was measured at 0 mV and is plotted vs. pH in Figure 3.3.

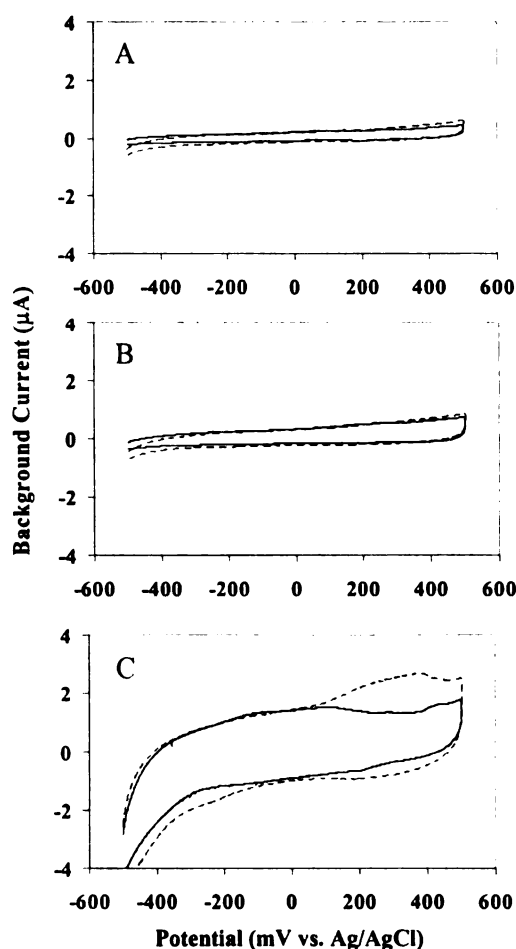


Figure 3.2. Cyclic voltammetric i -E curves for (A) microcrystalline diamond, (B) nanocrystalline diamond, and (C) GC electrodes in 0.1 M phosphate buffer, pH 2 (---) and pH 7 (—). Scan rate = 100 mV/s . Electrode geometric area = 0.16 cm^2 .

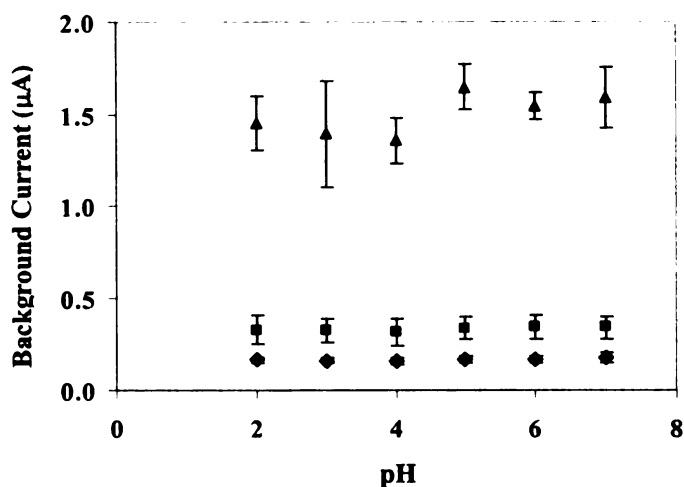


Figure 3.3. Background current measured at 0 mV vs. pH for microcrystalline diamond (◆), nanocrystalline diamond (■), and GC (▲) electrodes in 0.1 M phosphate buffer. Scan rate = 100 mV/s. Electrode geometric area = 0.16 cm². Each data point and error bar represent the average and standard deviation of three measurements.

The magnitude of the background current for GC is about ten times greater than that for microcrystalline diamond and about five times greater than that for nanocrystalline diamond. A low background current is a common property of diamond electrodes and lead to improved S/B and signal-to-noise (S/N) ratios in electroanalytical measurements. There are three causes for the low background current at diamond. First, compared to GC, there is much less contribution to the background current from electroactive carbon-oxygen functionalities (pseudocapacitance) since the diamond surface is hydrogen-terminated. GC contains surface carbon-oxygen functionalities, some of which are electroactive (e.g., quinones/hydroquinones).⁵³ The increased background current for GC is also due to ionizable surface carbon-oxygen functionalities (e.g., carboxylic acid), which are charged at pH above their pK_a and may interact with electrolyte ions.⁵¹ Second, the semimetal-semiconductor nature of the diamond electrode

causes a slightly lower density of surface electronic states near the Fermi level. The lower surface charge density leads to a reduced accumulation of charge on the solution side of the interface (e.g., double-layer charging). Third, the diamond surface may be structured as an array of microelectrodes, with conductive regions isolated from more insulating regions.¹⁷

The background current for both diamond types is independent of the solution pH, consistent with the absence of ionizable surface carbon-oxygen functionalities. The background current for nanocrystalline diamond is larger than that for microcrystalline diamond presumably because of the increased fraction of exposed grain boundary. The π -bonded carbon in the grain boundaries is a source of charge carriers which can increase the capacitive component of the background current. Some of these carbons may contain electrochemically active surface carbon-oxygen functionalities which would give rise to a faradaic component in the background current.³⁶

As evident in Figure 3.2, the cyclic voltammetric *i*-*E* curves for both diamond types are featureless with no evidence for any surface redox chemistry. For GC at pH 2, broad oxidation and reduction peaks are present between 200 and 400 mV. These peaks are associated with redox-active surface carbon-oxygen functionalities. During polishing, carbon-carbon bonds are cleaved, leaving dangling bonds on the surface. Upon air exposure, atmospheric oxygen or water may react with the dangling carbon bonds to form surface carbon-oxygen functional groups.⁵⁴ Some of the resulting surface functional groups (e.g., hydroquinones/quinones) are electroactive and cause the background voltammetric features. The midpoint potential for the redox peaks shift negative with increasing pH, but the peaks are not as prominent as they are in acidic

media. The peaks shift negatively with increasing pH with a charge of ca. -59 mV/pH unit. This is consistent with equal numbers of protons and electrons being transferred. The data in Figure 3.3 illustrate the greater variability in the background current for GC than for diamond over this pH range. This difference is attributed to the pH-dependent electrochemical behavior of the electroactive carbon-oxygen surface functionalities. It is also evident that the standard deviation of the current for GC at all potentials is much larger than the deviation for the two diamond types. It can be difficult to reproduce the surface properties of GC during polishing, hence there is inherently some variability in the response. The fact that diamond electrodes do not require pretreatment for activation is an advantage for electroanalytical measurements. Figure 3.4 shows the cyclic voltammograms for GC in phosphate buffer at pH 2, 4, and 7 during a potential sweep from -200 to $+1200$ mV. Clearly, the redox peaks shift to more positive potentials with decreasing pH, and are most prominent at pH 2.

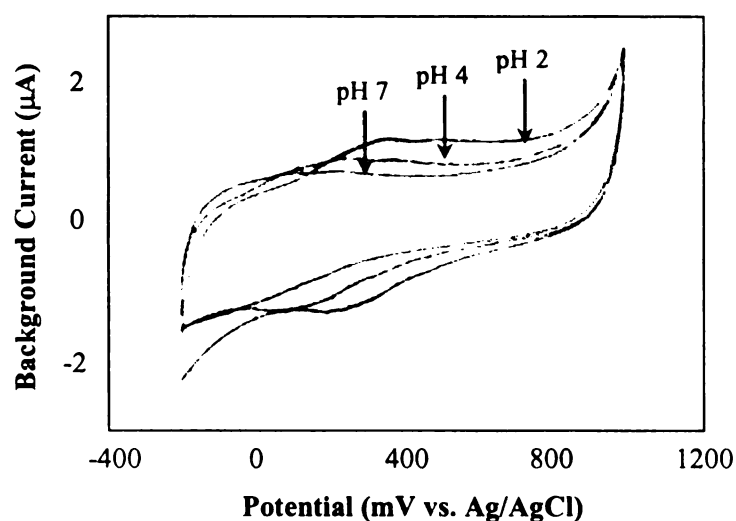


Figure 3.4. Cyclic voltammetric i - E curves for GC in 0.1 M phosphate buffer, pH 2, 4, and 7. Scan rate = 100 mV/s. Electrode geometric area = 0.16 cm².

The influential nature of the surface oxides on the magnitude of the background current and on the electrode reaction kinetics at sp^2 carbon electrodes has been discussed by other research groups.^{54,55} For example, Deakin et al. showed that the k°_{app} value for several outer-sphere redox system changed with pH.⁵⁶ The rate was found to decrease with increasing pH for $Fe(CN)_6^{-3/-4}$ and $IrCl_6^{-2/-3}$, and the opposite effect was observed for $Ru(NH_3)_6^{+2/+3}$. The behavior was consistent with the presence of functional groups on the GC surface. Runnels et al. reported on the effect of solution pH and surface functional groups on the voltammetric behavior of carbon fiber toward catecholamines.⁵⁴ The authors observed redox waves at the background voltammetric response that shifted and decreased in magnitude with increasing pH. The background voltammetric peaks for the surface oxides on carbon fiber overlap those for neurotransmitters like dopamine. Additionally, the electrode is quite responsive to the pH of the solution in contact with it. This is a problem in neurochemical investigations *in vivo* because simultaneous changes of dopamine after exocytosis and pH occur in brain tissue. Hydrogen-terminated diamond microelectrodes may be ideal for these types of applications because the background current is low and insensitive to pH changes.

The cyclic voltammetric response for 10 μ M solutions of DA, CAT, and DOPAC at microcrystalline diamond and GC are presented in Figures 3.5 and 3.6. Measurements were made at pH 2 to 7, with the electrodes being soaked in distilled IPA then rinsed copiously with ultrapure water between measurements. Data are presented for two different pH values, 7 and 2.

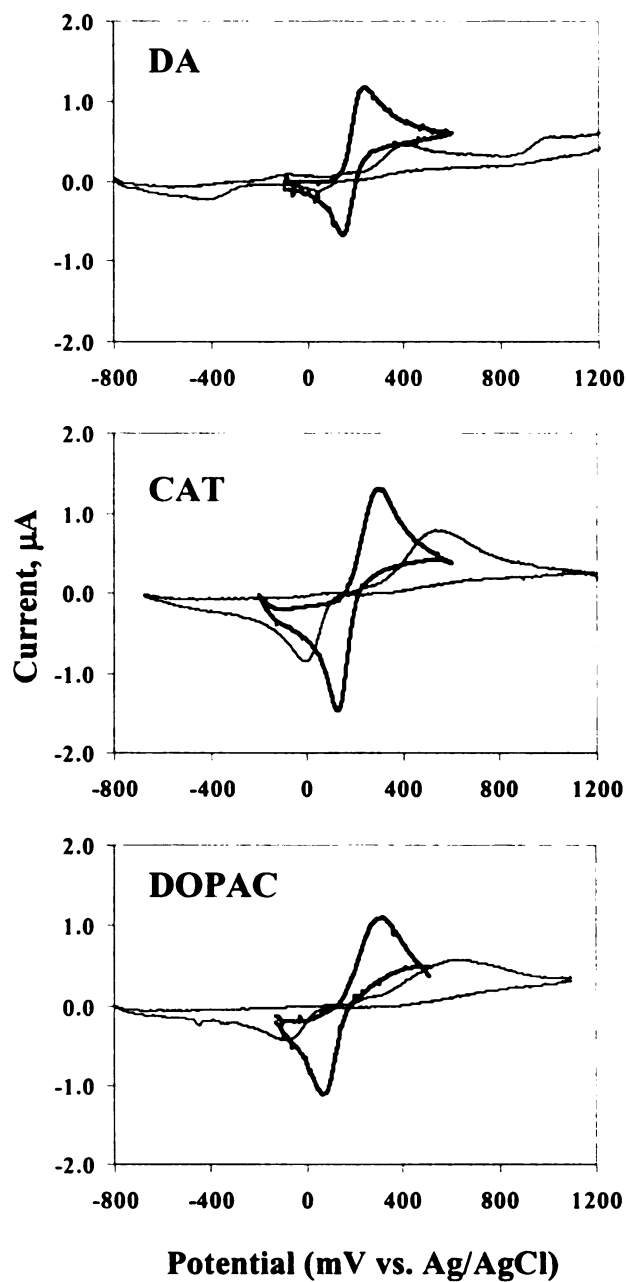


Figure 3.5. Cyclic voltammetric i-E curves (background-subtracted) for microcrystalline diamond (—) and GC (---) electrodes in 10 μ M DA, CAT, and DOPAC in 0.1 M phosphate buffer, pH 7. Scan rate = 100 mV/s. Electrode geometric area = 0.16 cm^2 .

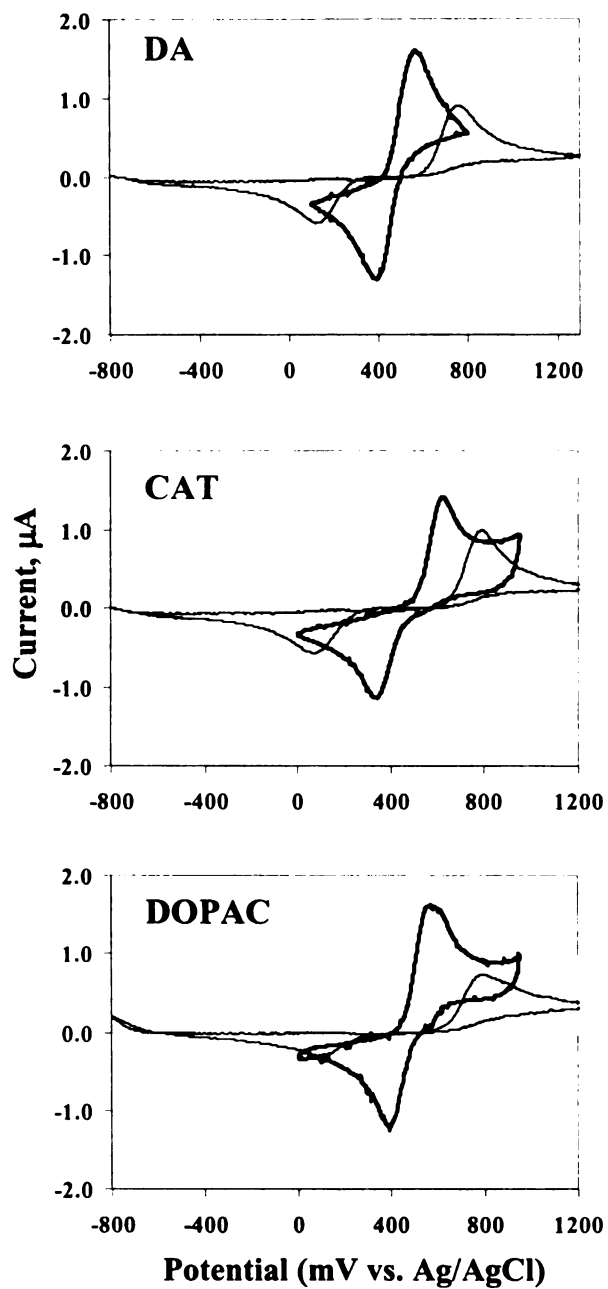


Figure 3.6. Cyclic voltammetric *i*-E curves (background-subtracted) for microcrystalline diamond (—) and GC (---) electrodes in 10 μ M DA, CAT, and DOPAC in 0.1 M phosphate buffer, pH 2. Scan rate = 100 mV/s. Electrode geometric area = 0.16 cm^2 .

The curves for DA at the diamond electrodes at pH 7 show peaks besides those that correspond to the dopamine quinone/hydroquinone redox reaction ($E_p^{ox} \sim 350$ mV and $E_p^{red} \sim 50$ mV). An extra pair of peaks at $E_p^{ox} \sim -225$ mV and $E_p^{red} \sim -260$ mV (data not shown) is also observed for GC when the potential is scanned more negative. The additional peaks and the quite low peak currents for duroquinone mean that there are other stable species formed during the electrode cycling. Duroquinone is a highly reactive species, and is susceptible to nucleophilic attack in the 6-position. The nucleophilic attack of aniline, cysteine, and glutathione has been observed.^{57,58} The most common nucleophilic addition is that of its own side-chain amine, producing 5,6-dihydroxyindoline which is also oxidizable.⁵⁹ Pertinent molecular structures are shown in Figure 3.7. The extra peaks are attributed to 5,6-dihydroxyindoline and its oxidation product. This intramolecular cyclization may only occur when there is sufficient unprotonated orthoquinone available to allow the side-chain amine to act as a nucleophile. Thus, the extra peaks were observed at pH 7, and to a lesser extent at pH 6.

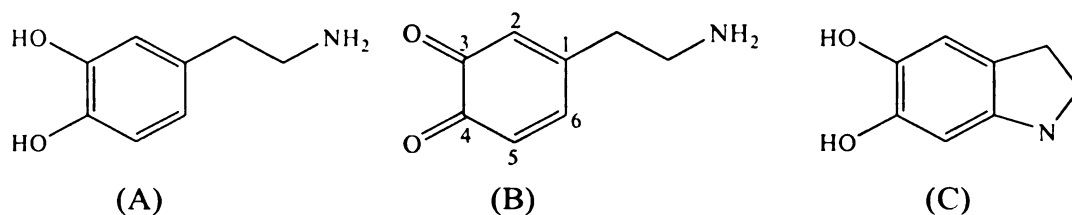


Figure 3.7. Dopamine (A) oxidizes to duroquinone (B). The 6-position is susceptible to nucleophilic attack by the side-chain amine forming 5,6-dihydroxyindoline (C).

The cyclic voltammetric peak current for reversible and irreversible systems is described by the Randles-Sevcik equation:⁶⁰

$$i_p = (2.69 \times 10^5) n^{3/2} A D^{1/2} C v^{1/2}$$

in which i_p is peak current (A), n is electron stoichiometry, A is electrode area (cm^2), D is diffusion coefficient (cm^2/s), C is concentration (mol/cm^3), and ν is scan rate (V/s). This equation relates the maximum current to various parameters when the reaction rate is limited by semi-infinite linear diffusion of reactant to the interfacial reaction zone. The peak currents at the three electrode types were found to vary linearly with the square root of the scan rate, $\nu^{1/2}$ ($R^2 > 0.99$) for all the analytes, which is indicative of diffusion control. Using $n = 2$, $A = 0.16 \text{ cm}^2$, $D = 6 \times 10^{-6} \text{ cm}^2/\text{s}$, $C = 1 \times 10^{-8} \text{ mol}/\text{cm}^3$, and $\nu = 0.1 \text{ V}/\text{s}$, i_p was calculated to be $0.96 \text{ }\mu\text{A}$. Figure 3.8 shows plots of i_p^{ox} vs. pH for microcrystalline diamond, nanocrystalline diamond, and GC in $10 \text{ }\mu\text{M}$ analyte solutions, the theoretical i_p value indicated by the dashed line. The i_p^{ox} values are lower at the two diamond types compared to that at GC over the entire pH range investigated. The larger current is attributed to preconcentration or adsorption of the analyte on GC. The catechol redox reaction on GC involves both adsorption and diffusion transport.

The present findings also indicate higher i_p^{ox} values on nanocrystalline than on microcrystalline diamond, for all the analytes at all pH, indicating some preconcentration of the analyte occurring on the electrode surface. Nanocrystalline diamond has more grain boundaries and thus a greater fraction of exposed sp^2 -bonded carbon which was reported to have a correlation with surface coverage of adsorbed catechols. Nanocrystalline diamond exhibits greater adsorption than microcrystalline diamond.³⁶

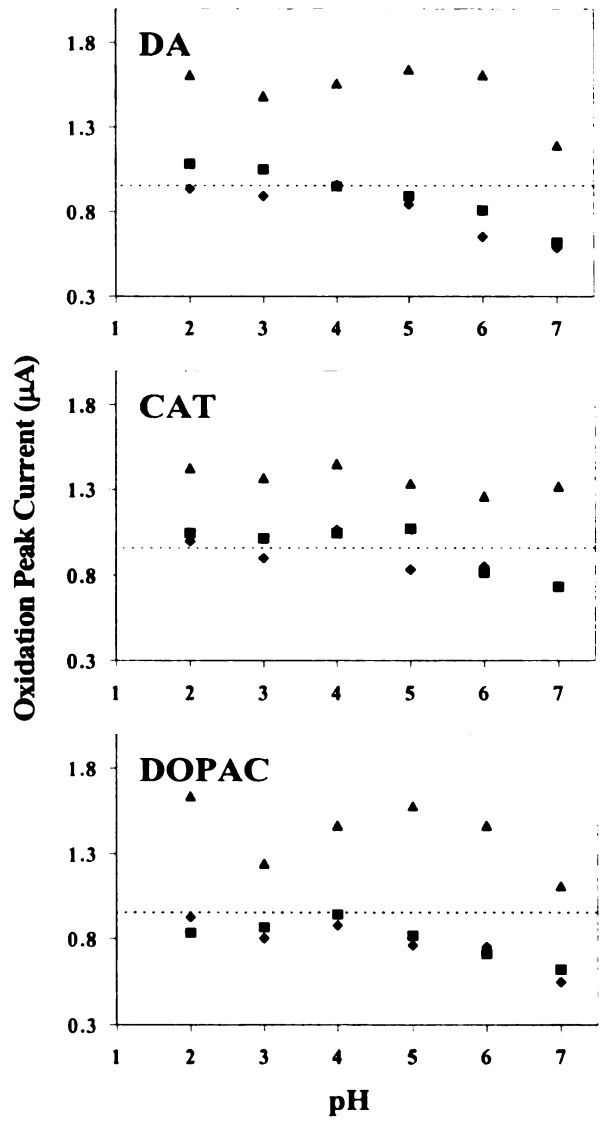


Figure 3.8. Plots of oxidation peak current vs. pH for microcrystalline diamond (\blacklozenge), nanocrystalline diamond (\blacksquare), and GC (\blacktriangle) electrodes in 10 μM DA, CAT, and DOPAC in 0.1 M phosphate buffer. Scan rate = 100 mV/s. Electrode geometric area = 0.16 cm^2 . The theoretical i_p value is indicated by the dashed line.

Figure 3.9 shows plots of E_p^{ox} vs. pH for DA, CAT and DOPAC at microcrystalline diamond, nanocrystalline diamond and GC. Such plots are often used to study the mechanism of an electrochemical redox reaction. Cyclic voltammetric investigations as a function of pH and in conjunction with mathematical treatment permit the determination of the order of the proton (H^+) and electron (e^-) transfers on platinum⁶¹ and carbon^{55,62,63} electrodes. For example, data on the kinetic studies of catechol oxidation at a carbon paste electrode at neutral pH were found to be consistent with an HeHe mechanism.⁵⁵ Such a comprehensive task was not pursued in this research but it is certainly interesting to make similar investigations with diamond electrodes.

E_p^{ox} values reflect the ease of oxidation, that is, high E_p^{ox} means that more driving force is needed for the electron transfer reaction between the solution analyte and the electrode. The higher E_p^{ox} values of the catechol compounds at diamond, as compared to that at GC, mean that the electrode reaction kinetics are more sluggish at the former. This means that more positive potentials are required to oxidize the catechols and catecholamines at diamond at a mass transfer-limited rate. This is not expected to hinder the performance of diamond as a detection electrode due to its wide working potential window and low background current.

Another important parameter to consider is the peak separation ($\Delta E_p = E_p^{ox} - E_p^{red}$), which is related to the heterogeneous rate constant. A large ΔE_p value is indicative of sluggish redox reaction kinetics. Table 3.1 shows the ΔE_p values for DA, CAT, and DOPAC at pH 7. Figure 3.9 and Table 3.1 show that E_p^{ox} and ΔE_p values follow the trend: microcrystalline diamond > nanocrystalline diamond > GC. The slow redox reaction rate on the diamond electrodes is presumably due to the relative absence of

The E_p^{ox} values of catechol compounds at diamond electrodes decrease with increasing pH. In addition, a trend based on the charge of the analyte emerges, in particular, higher E_p^{ox} values are observed for negatively-charged analytes and lower for those which are positively-charged. At pH 2, 3, and 4, when DOPAC is predominantly protonated (neutral), E_p^{ox} is lowest for DA followed by DOPAC then by CAT. The E_p^{ox} of DOPAC and CAT are almost equal at pH 5, right above the pK_a of DOPAC. At pH 6 and 7, when the unprotonated form of DOPAC (negatively-charged) is dominant, the E_p^{ox} values follow the order $DA < CAT < DOPAC$. The ΔE_p values for DA, CAT, and DOPAC at pH 7 also show charge discrimination on the three electrodes. Fastest electron transfer, as evidenced by the least positive E_p^{ox} , is observed for DA and slowest electron transfer is seen for DOPAC. The general trends in the E_p^{ox} values at varying pH that are observed on GC are also seen on diamond. Considering the disparity in their electrode surface chemistries, a greater dissimilarity of the trends in the electron transfer kinetics of the analytes on GC and on diamond is expected.

A trend based on analyte charge is an indication that an electrostatic mechanism is in effect. The results presented for GC agree with previously published work,⁶⁵ that is, that the rate of electron transfer is dependent on the analyte charge. The redox reaction is fastest for the positively-charged DA and slowest for the negatively-charged DOPAC. The electron transfer kinetics are governed by electrostatic interactions between the analytes and the electrode surface. DA kinetics are enhanced while that of DOPAC are inhibited since the surface oxides are neutral or anionic, and never cationic.⁵¹ On the diamond surface, an electrostatic mechanism is unanticipated but is apparent.

adsorption. An increased electron transfer rate (lower E_p^{ox} and ΔE_p values) at nanocrystalline diamond compared to microcrystalline diamond is observed. This is another evidence of the occurrence of adsorption through the sp^2 -bonded carbon on the grain boundaries of the nanocrystalline diamond surface.

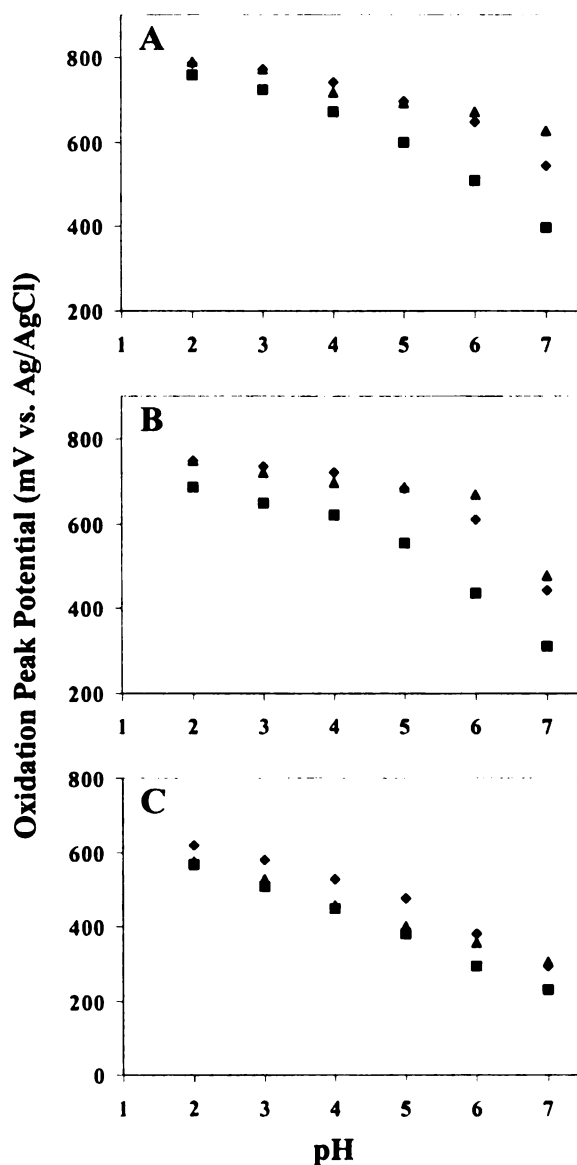


Figure 3.9. Plots of oxidation peak potential vs. pH for (A) microcrystalline diamond, (B) nanocrystalline diamond, and (C) GC electrodes in 10 μ M solutions of DA (■), CAT (◆), and DOPAC (▲) in 0.1 M phosphate buffer. Scan rate = 100 mV/s. Electrode geometric area = 0.16 cm².

Table 3.1. ΔE_p values of the catechol compounds at pH 7 at the three electrode types.

	ΔE_p (mV)		
	DA	CAT	DOPAC
Microcrystalline Diamond	353	547	711
Nanocrystalline Diamond	233	422	516
Glassy Carbon	81	168	233

Note: 10 μ M solutions of the analytes in 0.1 M phosphate buffer, pH 7 was used. Scan rate = 100 mV/s. Electrode geometric area = 0.16 cm².

Investigations done by McCreery's group indicate that adsorption of the catechols to the carbon electrode surface is necessary for an increased electron transfer rate. It was found that surface pretreatments that inhibit adsorption result in high ΔE_p and those that promote adsorption lead to low ΔE_p values.⁶⁴ Their findings led to a self-catalysis mechanism in which a layer of adsorbed quinones (physisorbed or chemisorbed quinone or catechol) catalyzes the electron transfer between catechols and GC electrodes. Hydrogen-bonding between a surface quinone oxygen and the catechol is a possible catalytic step that can accelerate the overall redox process.⁵² Adsorption and fast electron transfer translate to sharper peaks and higher peak currents.⁵¹

For sp² carbon electrodes, a trade-off exists between the electrode's enhanced sensitivity through fast electron transfer kinetics and its susceptibility to polar adsorbates that lead to fouling and decreased activity. Little is known about electron transfer reaction mechanism of these compounds. A better understanding of the redox reaction mechanism and the factors that affect the redox reaction rate on diamond would be beneficial for improving the sensitivity and fouling resistance of this material in electrochemical detection.

It is possible that surface oxides may have also played a role in the case of diamond electrodes. Electrochemically generated carbon-oxygen functional groups may have resulted from the wide potential sweeps used to drive the redox reaction on diamond. Change in diamond surface termination from hydrogen to oxygen have been reported to occur at applied potentials as low as 1.0 V vs. SCE in acidic media.⁶⁶ Angus and coworkers have attributed a redox couple observed at 1.7 V vs. SHE to surface oxidation.²¹ Fujishima et al. used anodic treatment to replace surface hydrogen with oxygen functionalities to achieve improved selectivity between DA and ascorbic acid.⁶⁷ Figure 3.10 shows possible oxygen functional groups found on sp^2 and sp^3 electrode surfaces.⁶⁸ It is important to note that the oxidation of diamond differs from that of sp^2 carbon electrodes in that the reactions are surface-confined and do not produce any morphological and microstructural damage on diamond owing to the strong three-dimensional bonding and high atomic density of diamond.⁶⁶

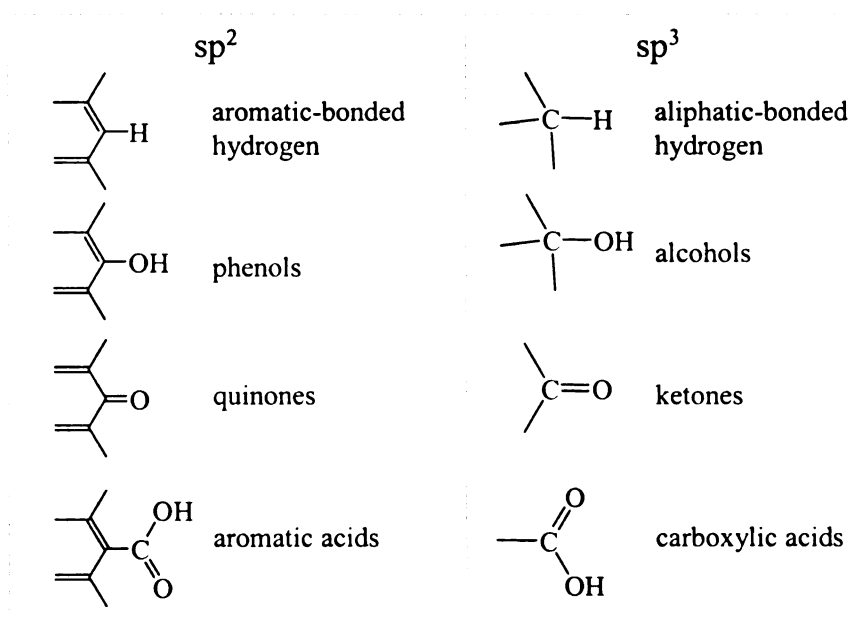


Figure 3.10. Surface functional groups on oxidized sp^2 and sp^3 electrodes.

Three trials were performed to determine the reproducibility of the cyclic voltammetric measurements of the analytes on the three electrode types. Cyclic voltammetry was performed at $\nu = 100$ mV/s, and $A = 0.16$ cm², with 0.1 M phosphate buffer as the supporting electrolyte. The RSD values on the E_p^{ox} and i_p^{ox} values are tabulated in Table 3.2. The high RSD values for GC shows the difficulty in obtaining polished GC surfaces with reproducible electrode characteristics. The microcrystalline diamond films used were grown in one batch resulting to lower RSD values compared to that of the nanocrystalline diamond films which were grown individually.

Table 3.2. Reproducibility of the cyclic voltammetric measurements using the three electrode types being studied (n = 3).

	RSD		Analyte
	E_p^{ox}	i_p^{ox}	
Microcrystalline Diamond	1.4%	1.3%	5 μ M CAT, pH 2
Nanocrystalline Diamond	3.9%	10.9%	5 μ M CAT, pH 2
Glassy Carbon	8.5%	17.1%	10 μ M DA, pH 7

The supporting electrolyte used was 0.1 M phosphate buffer. Scan rate = 100 mV/s. Electrode geometric area = 0.16 cm².

3.2. Amperometric Detection of Catechols and Catecholamines in Flow Injection Analysis

3.2.1. Introduction

It was shown in the previous section that catechols and catecholamines can be electrooxidized at boron-doped microcrystalline and nanocrystalline diamond thin films, albeit with higher overpotential than GC. The results presented in this section

demonstrate the capability of diamond electrodes for the oxidative detection (amperometric mode) and quantification of these analytes when coupled with flow injection analysis (FIA). The goal of the work was to compare the performance of both microcrystalline and nanocrystalline diamond thin films with that of GC. A comprehensive reporting of the detection figures of merit is presented.

FIA was conceived in the mid-1970s in order to process large numbers of samples for analysis. FIA was developed as a solution to the slow productivity resulting from the use of segmented flow analyzers (SFA).⁶⁹ The FIA technique is based on the injection of a sample in a continuously flowing, nonsegmented carrier solution propelled by a peristaltic pump. The injected sample forms a well-defined zone, which is then transported through the detector. In one mode of operation, a detector continuously records a physical parameter, such as absorbance (fixed wavelength) or electrode current (fixed potential), and its change due to passage of the sample zone. The output is a detector signal as a function of time, which can be used for quantitative analysis (peak height or area).^{70,71} The benefits of FIA include automated sample processing, high repeatability, short analysis time, adaptability to microminiaturization, containment of chemicals, and waste reduction.^{72,73} FIA is more analogous to modern HPLC than to SFA, such that it has been called "HPLC without the column and high pressures".⁷³

Electrochemical detection relies on a compound undergoing oxidation or reduction at an electrode to which a potential has been applied. The amperometric detection mode provides the advantage of minimizing the charging current by operating at a fixed potential as opposed to voltammetric techniques. The electrochemical flow cell acts as the transducer between the potentiostat and the FIA or HPLC system. A wide

range of electrochemical cell designs have been used for flowing streams. The cell design must have a high S/N ratio, low dead volume, well-defined hydrodynamics, small ohmic drop, and ease of construction and maintenance.⁴⁹

The thin-layer cell is probably the most popular detector cell configuration. A schematic of the homemade thin-layer flow cell used in this work was presented in Chapter 2. A simple diagram is presented in Figure 3.11 to illustrate the solution flow with respect to the working electrode. The carrier solution in FIA-EC and the mobile phase in HPLC-EC act as the supporting electrolyte. Electrochemistry proceeds while a thin layer of solution flows parallel across the planar electrode surface, which is imbedded in a rectangular channel. Mass transfer occurs not only through diffusional transport to the electrode surface, but also through forced convection due to the fluid flow, hence electrochemistry applied to flowing streams is classified as a hydrodynamic technique. The enhanced mass transfer translates to higher currents and thus higher S/N ratios.^{49,74} The conversion efficiency, that is the amount of analyte electrolyzed as it is swept past the electrode, is typically less than 5% in this design.⁷⁵

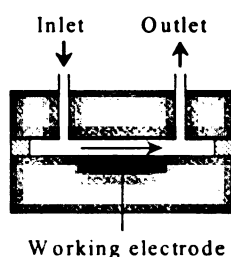


Figure 3.11. The solution flow in a thin-layer electrochemical flow cell.

FIA coupled with amperometric detection was used to assess the performance of boron-doped diamond for the measurement of catechols and catecholamines. The figures of merit used for this evaluation are the linear dynamic range, sensitivity, limit of

quantitation, and response precision. In addition, the response stability and the resistance to fouling by a biomolecule were evaluated.

3.2.2. Results and Discussion

Hydrodynamic voltammetric background i-E curves for microcrystalline diamond, nanocrystalline diamond and freshly polished GC in 0.1 M phosphate buffer with 0.1 M NaCl, pH 7.2, are shown in Figure 3.12. The carrier solution volumetric flow rate (U) was 1.0 mL/min. The curves were obtained by changing the applied potential in 100-mV increments starting at 200 mV. The current magnitude and the peak-to-peak noise were recorded once a stable signal was reached.

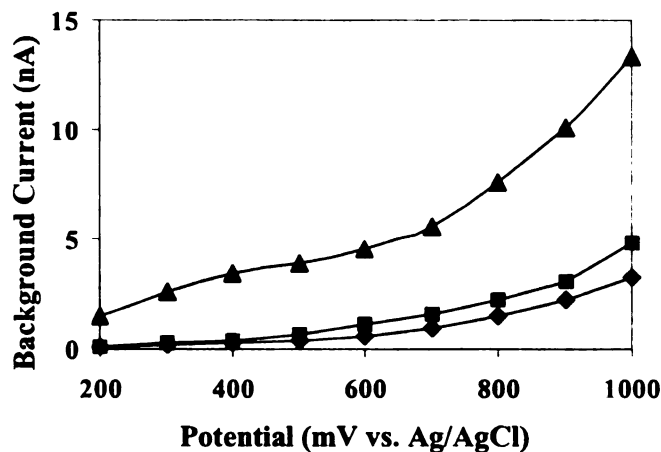


Figure 3.12. FIA-EC hydrodynamic voltammetric background i-E curves for microcrystalline diamond (◆), nanocrystalline diamond (■), and GC (▲) electrodes in 0.1 M phosphate buffer, 0.1 M NaCl, pH 7.2. Flow rate = 1.0 mL/min. Electrode geometric area = 0.12 cm².

After application of a detection potential, the background current for the diamond films stabilized much faster than did the current for GC. For example, a stable

background current was easily reached within 10 min for the diamond films, while 40 min was required for GC at 700 mV. The quick stabilization time for diamond is expected due, in part, to the low double-layer capacitance. Additionally, the diamond surface is morphologically and microstructurally stable at anodic potentials so no dynamic oxidation processes or microstructural alteration occur on the surface. Surface oxidation does occur on diamond but is confined to a simple functional group exchange on the surface.⁶⁶ The rapid stabilization time of diamond leads to shorter overall analysis times.

As was the case in the cyclic voltammetric measurements, the background current is larger for GC than for the two diamond types. A low background current, as discussed in the previous section, is a characteristic feature of diamond electrodes. For example, the anodic background current at 400 mV was 0.24, 0.41, and 3.40 nA for microcrystalline diamond, nanocrystalline diamond, and GC, respectively. All electrodes had the same exposed geometric area. The rapid rise in background at potentials above 700 mV for GC is likely due to a combination of surface oxidation and onset of oxygen evolution. The low background current on diamond leads to an enhanced S/B ratio.

Figure 3.13 shows the peak-to-peak noise for the three electrode types as a function of applied potential. The noise levels are significantly lower for both diamond types at potentials less than 800 mV, with the lowest noise seen for microcrystalline diamond. At potentials positive of 800 mV, the noise levels start to be more comparable, especially for the nanocrystalline diamond and GC electrodes. The lower noise levels for diamond lead to improved S/N ratios in electroanalytical measurements and lower limits of detection.

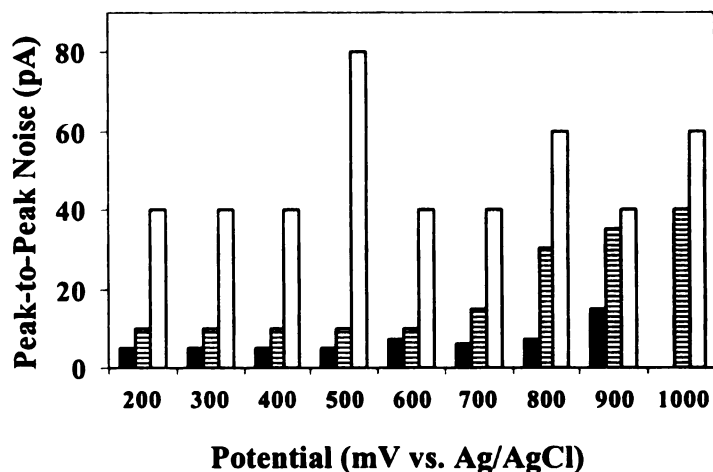


Figure 3.13. Peak-to-peak noise at microcrystalline diamond (■), nanocrystalline diamond (▨), and GC (□) electrodes in 0.1 M phosphate buffer, 0.1 M NaCl, pH 7.2, as a function of applied potential. Flow rate = 1.0 mL/min. Electrode geometric area = 0.12 cm².

Figure 3.14 shows hydrodynamic voltammetric *i*-*E* curves for 20 μL injections of CAT, MC, BC, NE, EP, DA, and DOPAC, all 30 μM, at microcrystalline diamond, nanocrystalline diamond, and GC electrodes. These curves were obtained by making multiple injections (*n* ≥ 4) of each analyte at different applied potentials. The error bars are within the size of the marker. The resulting hydrodynamic *i*-*E* curves generally have well-defined, sigmoidal profiles with mass transport limited currents. The limiting current for a thin-layer flow cell is described by the equation:⁴⁹

$$i_{lim} = 1.47nFC(DA/b)^{2/3}U^{1/3}$$

where i_{lim} is the limiting current (A), n is electron stoichiometry, F is the Faraday constant, C is concentration (mol/cm^3), D is diffusion coefficient (cm^2/s), A is electrode area (cm^2), b is channel height (cm), and U is average volume flow rate (cm^3/s). Calculation of i_{lim} , using $n = 2$, $C = 3 \times 10^{-8} \text{ mol}/\text{cm}^3$, $D = 6 \times 10^{-6} \text{ cm}^2/\text{s}$, $A = 0.12 \text{ cm}^2$, $b = 0.075 \text{ cm}$, and $U = 0.017 \text{ cm}^3/\text{s}$, gives a value of $0.98 \mu\text{A}$. The experimental results reveal currents all lower than this theoretical value. One possible reason for this is the error in the value of b in the flow cell. A rubber gasket compression of 25% that was used in the calculation is an estimate. There is always some uncertainty in b because the actual channel height is a factor of the degree of compression, which is a function of how tightly the screw clamp is made to hold the top and bottom pieces of the flow cell together.

The optimum detection potentials (E_{det}) and oxidation half-wave potentials ($E_{1/2}$) are tabulated in Table 3.3. The E_{det} is selected to be in the limiting current region. Potentials in this region yield the most intense current and at these potentials the electrode sensitivity is not greatly affected if the potentials happen to drift. Higher potentials are required to detect the catechols and catecholamines at diamond, as previously discussed. Fortunately, the more positive detection potential required for diamond is not a significant detriment to the electrode performance due to the fact that the microstructure and morphology are stable, which results in the maintenance of low and stable background currents.

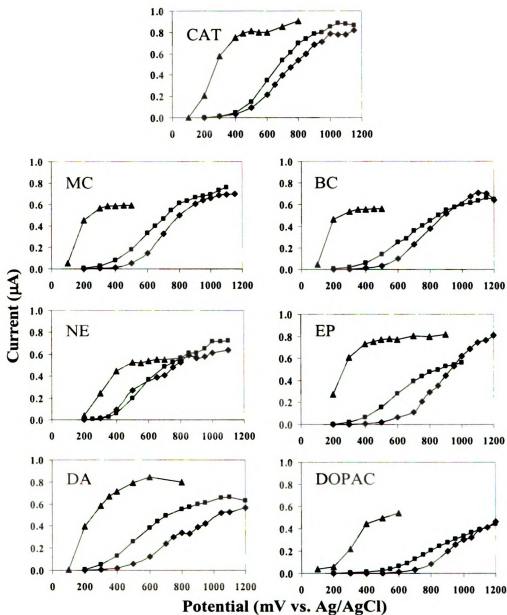


Figure 3.14. Hydrodynamic voltammetric i-E curves for 20 μL injections of 30 μM catechols and catecholamines in microcrystalline diamond (\blacklozenge), nanocrystalline diamond (\blacksquare), and GC (\blacktriangle). The carrier solution was 0.1 M phosphate buffer, 0.1 M NaCl, pH 7.2. Scan rate = 1.0 mL/min. Electrode geometric area = 0.12 cm^2 .

Table 3.3. E_{det} and $E_{1/2}$ values for the amperometric detection of the analytes at microcrystalline diamond, nanocrystalline diamond, and GC.

Analyte	E_{det} (mV vs. Ag/AgCl)			$E_{1/2}$ (mV vs. Ag/AgCl)		
	Micro-crystalline Diamond	Nano-crystalline Diamond	GC	Micro-crystalline Diamond	Nano-crystalline Diamond	GC
CAT	1100	1000	500	700	650	250
MC	1000	950	350	750	650	150
BC	1150	1050	350	800	650	150
NE	950	900	550	550	550	350
EP	1150	850	450	850	600	250
DA	1150	850	400	700	550	200
DOPAC	1150	850	450	900	800	350

There are several trends evident in the hydrodynamic voltammetric data. First, there is a difference in the electrode reaction kinetics for these catechols and catecholamines as the $E_{1/2}$ becomes more positive in the following order: GC < nanocrystalline diamond < microcrystalline diamond. The more sluggish kinetics for this class of redox analytes at diamond is well known. The electrode reaction kinetics are presumed to be slower on the diamond electrodes because of a lack of adsorption. Second, sigmoidal voltammetric peaks are seen for all the analytes with limiting currents that are similar for a given analyte at all three electrodes. This observation is different from the cyclic voltammetric data in which the oxidation and reduction peak currents were consistently larger for GC, attributed to preconcentration or adsorption of the analyte on the GC surface. Due to the short residence time in the flow cell brought about by convection, there may be less adsorption occurring. Also, the additional convective

mass transport leads to more uniform currents for all these electrodes. The data presented in Table 3.3 show that it would be difficult to distinguish the analytes from each other because the E_{det} and $E_{1/2}$ values are similar for each electrode type. For analysis of solutions containing these analytes, a separation step, such as liquid chromatography or capillary electrophoresis, is required prior to electrochemical detection for speciation.

In order to evaluate the effectiveness of diamond for the analysis of catechols and catecholamines, the analytical detection figures of merit (i.e., response precision, sensitivity, linear dynamic range, limit of quantitation, and response stability) were obtained and compared with those for GC. The response precision was evaluated from a run of twenty consecutive 20- μL injections of 30 μM analyte at 1.0-min intervals. Three runs were made with each electrode type. For the two diamond types, one electrode was used for each run, while for GC, one piece was used for all three runs with polishing done prior to each run. Table 3.4 presents the data for the response precision reported as the % RSD, averaged from the three runs on each electrode type. The RSD values range from 1.4 to 2.4% for microcrystalline diamond, 1.2 to 2.0% for nanocrystalline diamond, and 1.5 to 5.0% for GC. The % RSD values between runs were also calculated and the values ranged from 5 to 50%. The variance in the degree of compression which affects the channel height is likely to be a major contributing factor in the run-to-run variability as the flow cell had to be disassembled and reassembled between runs to put a different test electrode in place.

Table 3.4. Response precision (% RSD) for catechol and catecholamine detection at microcrystalline diamond, nanocrystalline diamond, and GC in 0.1 M phosphate buffer, 0.1 M NaCl, pH 7.2.

Analyte	Microcrystalline Diamond	Nanocrystalline Diamond	Glassy Carbon
CAT	1.4	1.3	1.7
MC	1.5	1.3	1.8
BC	1.9	1.2	1.7
NE	2.4	1.4	2.9
EP	1.5	1.2	1.5
DA	1.5	1.9	2.5
DOPAC	2.1	2.0	5.0

Note: The response precision was evaluated from 20 consecutive injections at 1.0-min intervals. The data are reported as a mean for 3 runs. Analyte concentration = 30 μM . Injection volume = 20 μL . Flow rate = 1.0 mL/min. Electrode geometric area = 0.12 cm^2 . The detection potential used is as tabulated in Table 3.3.

Calibration curves for each of the analytes were generated from the detector response as a function of the concentration in order to determine the response sensitivity. Characteristic plots are shown in Figure 3.15. The curves are constructed from at least 5 concentrations with the lowest being the limit of quantitation (LOQ). The injected volume was 20 μL and the carrier solution flow rate was 1.0 mL/min. The calibration curves indicate that the current response increases linearly with analyte concentration for all the catechols and catecholamines tested at all three electrode types, each plot having $R^2 > 0.99$ and a near-zero y-axis intercept. The slope of these curves is the electrode sensitivity. The sensitivity is influenced, among other things, by the number of electrons involved in the redox reaction and electrode area.¹²

The linear dynamic range, LOQ, and the sensitivity for the catechols and catecholamines at all three electrode types are summarized in Table 3.5. The linear dynamic range for all the analytes studied, at all three electrode types, is 6 - 7 orders of magnitude ranging from the nM to mM range. The mass LOQ for all the analytes are similar, at all three electrode types, ranging from 10 to 80 pg. The sensitivity values for all the analytes at all three electrode types are also similar with values in the 10 – 30 nA/ μ M range.

The detection figures of merit presented in Tables 3.4 and 3.5 indicate that the diamond electrode performance is comparable to that of GC, albeit without any time-consuming pretreatment. The advantages of diamond in this electrochemical assay are (i) the rapid stabilization time after detector turn-on which leads to shorter overall analysis times, (ii) low background current and peak-to-peak noise resulting in high S/B and S/N ratios, and (iii) good electrode performance without the need for pretreatment for reactivation. The frequent polishing needed for GC is not only a tedious and lengthy procedure but is likely a cause of increased variability between measurements. Dismantling of the flow cell is necessary to gain access to the electrode for pretreatment. During reassembly of the flow cell, as discussed previously, differences in the channel height result from the different degrees of the compression of the rubber gasket.

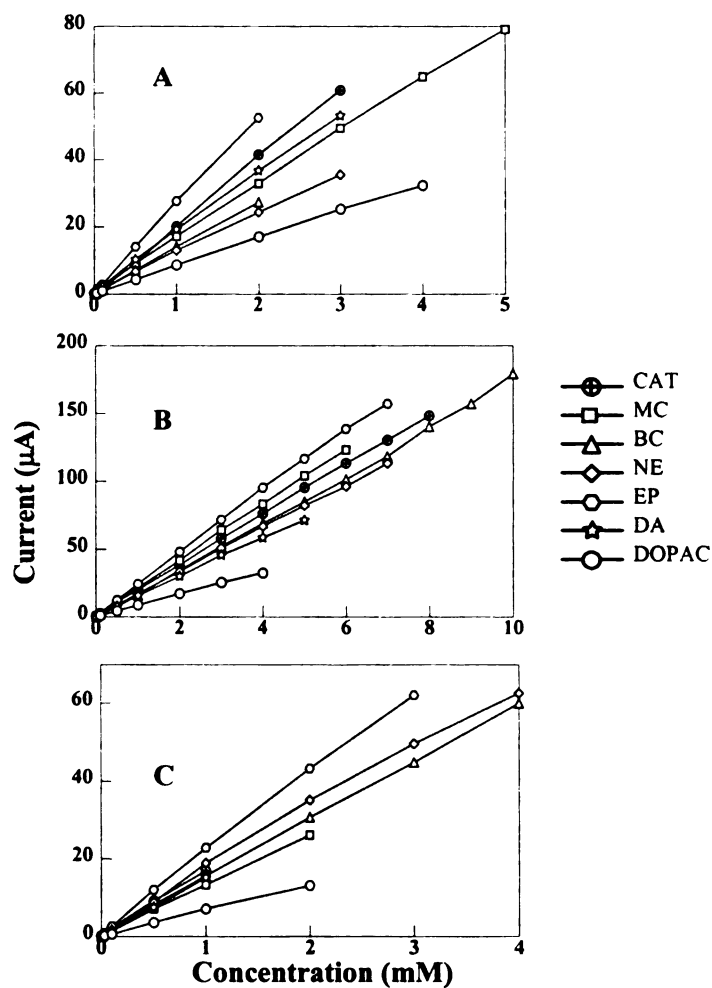


Figure 3.15. Calibration curves for the catechols and catecholamines obtained at (A) microcrystalline diamond, (B) nanocrystalline diamond, and (C) GC electrodes. Note: At least 5 concentrations were used for each curve but some plots appear to have fewer points because more measurements were made at the low μM level. The carrier solution was 0.1 M phosphate buffer, 0.1 M NaCl, pH 7.2. Flow rate = 1.0 mL/min. Injected volume = 20 μL . Electrode geometric area = 0.12 cm^2 .

Table 3.5. FIA-EC data for catechol and catecholamine detection at microcrystalline diamond, nanocrystalline diamond, and GC electrodes.

Analyte	Linear Dynamic Range	Sensitivity [†] (nA/μM)	LOQ at S/N ≥ 3
<i>Microcrystalline Diamond</i>			
CAT	10 nM - 3 mM	19 ± 4	22 pg
MC	10 nM - 5 mM	17 ± 3	25 pg
BC	10 nM - 2 mM	17 ± 8	33 pg
NE	10 nM - 3 mM	15 ± 6	34 pg
EP	20 nM - 2 mM	27 ± 9	73 pg
DA	10 nM - 3 mM	17 ± 5	38 pg
DOPAC	20 nM - 5 mM	11 ± 7	67 pg
<i>Nanocrystalline Diamond</i>			
CAT	5 nM - 9 mM	19 ± 7	11 pg
MC	20 nM - 6 mM	21 ± 9	50 pg
BC	10 nM - 10 mM	17 ± 6	33 pg
NE	10 nM - 7 mM	17 ± 7	34 pg
EP	10 nM - 7 mM	24 ± 3	37 pg
DA	10 nM - 5 mM	16 ± 9	38 pg
DOPAC	10 nM - 4 mM	9 ± 4	34 pg
<i>Glassy Carbon</i>			
CAT	5 nM - 1 mM	20 ± 5	11 pg
MC	20 nM - 2 mM	13 ± 7	50 pg
BC	10 nM - 4 mM	12 ± 9	33 pg
NE	10 nM - 4 mM	17 ± 1	34 pg
EP	10 nM - 3 mM	19 ± 4	37 pg
DA	10 nM - 1 mM	17 ± 4	38 pg
DOPAC	10 nM - 2 mM	10 ± 6	34 pg

[†] The data are based on the response of three electrodes and are reported at 95% confidence level. Correlation coefficients, R^2 , on the response curves are > 0.99.

Another series of experiments was performed to evaluate the diamond electrode response stability and resistance to fouling. The FIA-EC response for 20 μL injections of 2 mM NE at microcrystalline diamond, nanocrystalline diamond and GC electrodes was recorded over a 7-h period. Ten injections were made each hour with a Kreb's buffer, pH 7.4, flowing continuously at 1.0 mL/min for the entire duration of the experiment. The results are shown in Figure 3.16. Each data point represents the average of 10 injections. The error bars are within the size of the marker.

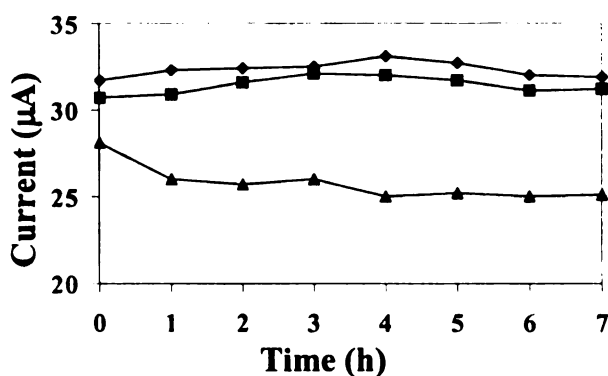


Figure 3.16. FIA-EC response for 20- μL injections of 2 mM NE at microcrystalline diamond (\blacklozenge), nanocrystalline diamond (\blacksquare), and GC (\blacktriangle) recorded over a 7-h period. The carrier solution was a Kreb's buffer, pH 7.4, flowing at 1.0 mL/min. Electrode geometric area = 0.12 cm^2 . Each data point shown represents an average of 10 injections made at 1.0 min intervals.

The current response over the period is quite stable for the two diamond types, while the response for GC decreases over the period before reaching a relatively constant value after approximately 4 h. At the end of the 7-h period, the current for GC decreased by 11% while that of microcrystalline diamond and nanocrystalline diamond changed by only 1% and 2%, respectively. Diamond possesses a better response stability than GC, in part, because of the morphological and microstructural stability of the material at the

detection potentials. The nonpolar, hydrogenated surface of diamond is also more resistive than the polar, oxidized GC surface to contaminant adsorption. As a result, diamond electrodes can be exposed to the laboratory atmosphere for days without any response attenuation while GC needs to be polished prior to each use in order to remove adsorbed contaminants and activate the electrode for electron transfer. The diamond electrodes are copiously rinsed with ultrapure water prior to placing in the flow cell. No response attenuation was observed during the course of an electrode performance evaluation which usually lasts for 2 – 3 days.

Figure 3.16 shows a GC current response markedly lower than that for the two diamond types. This is unexpected based on the comparable sensitivity values on the three electrodes as presented in Table 3.4. Possible explanations for this observation are the varying electrode activity that may result from each polishing and the varying channel height.

The resistance of diamond electrodes to fouling was further investigated by comparing the response for NE with and without added bovine serum albumin (BSA). Serum albumin is a good test interferent because it makes up 60% of the total plasma proteins in humans⁷⁶ and it readily and irreversibly adsorbs to oxidized carbon surfaces. Results for the two diamond types and GC are shown in Figure 3.17. The current responses for ten 20- μ L injections of 1 μ M NE were recorded at 1.0-min intervals and are represented by injection numbers 1 - 10. This was followed by another set of ten 20- μ L injections with 1 mM BSA added and are represented by injection numbers 11 - 20. A 17% decrease in current response of GC is observed when BSA is present. The GC response exhibits a gradual loss of signal with increasing injection number of the BSA-

containing solution. The response attenuation is about two times greater than that observed for the two diamond types, both of which showed an 8% decrease in response. Although there is some fouling for the two diamond types, the extent of fouling is less than that for GC. Adsorbed contaminants can be easily removed from the diamond surface by rinsing with ultrapure water, or in severe cases, by soaking in distilled IPA.

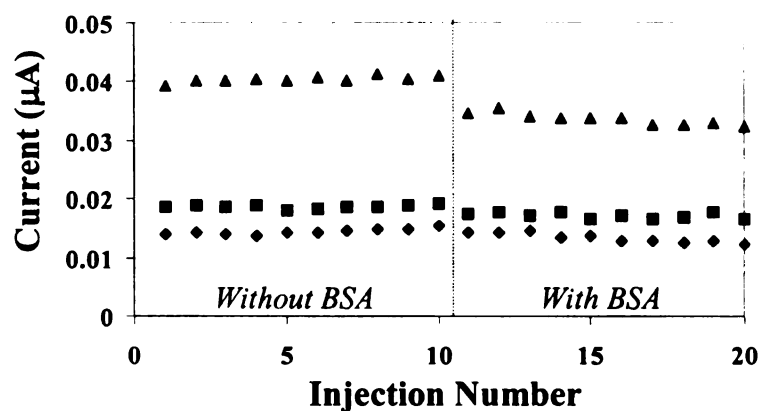


Figure 3.17. FIA-EC response for 20- μ L injections of 1 μ M NE (injections 1-10) and 1 μ M NE with 1 mM BSA (injections 11-20) at microcrystalline diamond (◆), nanocrystalline diamond (■), and GC (▲) electrodes. The carrier solution was a Kreb's buffer, pH 7.4, flowing at 1.0 mL/min. Injections were made at 1.0 min intervals. Electrode geometric area = 0.12 cm².

In summary, the response stability of both diamond electrode types was shown to be superior to that of GC. This property is beneficial particularly for electroanalytical applications that require longer term use of an electrode with minimal loss of activity and those that necessitate exposure of the electrode to interfering biomolecules.

3.3. Conclusions

Cyclic voltammetry was used to investigate the electrochemical behavior of catechols and catecholamines at microcrystalline diamond, nanocrystalline diamond, and

GC electrodes. Both diamond types exhibited a lower and more stable background current and noise than did GC. The diamond electrodes also showed no evidence for electrochemically-active surface carbon-oxygen functionalities. The background voltammetric current for both diamond types exhibited very little variation with solution pH. These results are in contrast to those for GC. The pH-insensitivity of the background current for diamond is clearly an advantage of this electrode material, particularly for *in vivo* measurement of catecholamines.

Extra peaks in the cyclic voltammograms of DA on the three electrode types at pH 7 demonstrate that coupled intramolecular cyclization reaction occurs when the 6-position undergoes nucleophilic attack by the amine side-chain. Preconcentration of the analytes on the GC electrode surface due to adsorption is evident from the experimental i_p values that are higher than the theoretical value. Because the i_p^{ox} values demonstrated a linear relationship with $v^{1/2}$, mixed diffusion and adsorption control is presumed. The ΔE_p values for the two diamond types are larger than those for GC. For example, the ΔE_p values for DA at pH 7 are 353, 233, and 81 mV, for microcrystalline diamond, nanocrystalline diamond, and GC, respectively. A high ΔE_p value is indicative of sluggish redox reaction kinetics. The slow electron transfer kinetics of the catechol/orthoquinone system is attributed to the absence of adsorption. Hydrogen-bonding between the catechol and the adsorbed quinone or catechol layer adsorbed on the electrode surface is believed to be a catalytic step. The faster redox reaction rate at nanocrystalline compared to microcrystalline diamond is attributed to the greater fraction of sp^2 -bonded carbon which has been previously shown to give rise to an increased coverage of adsorbed catechols.

The values of E_p^{ox} at varying pH exhibited trends that are charge-based indicating electrostatic effects for all three electrode types. This outcome is unexpected on the hydrogen-terminated diamond surface, so the presence of surface oxides was suggested. Oxidation of the diamond surface may have occurred because wide potential sweeps were necessary to drive the redox reaction.

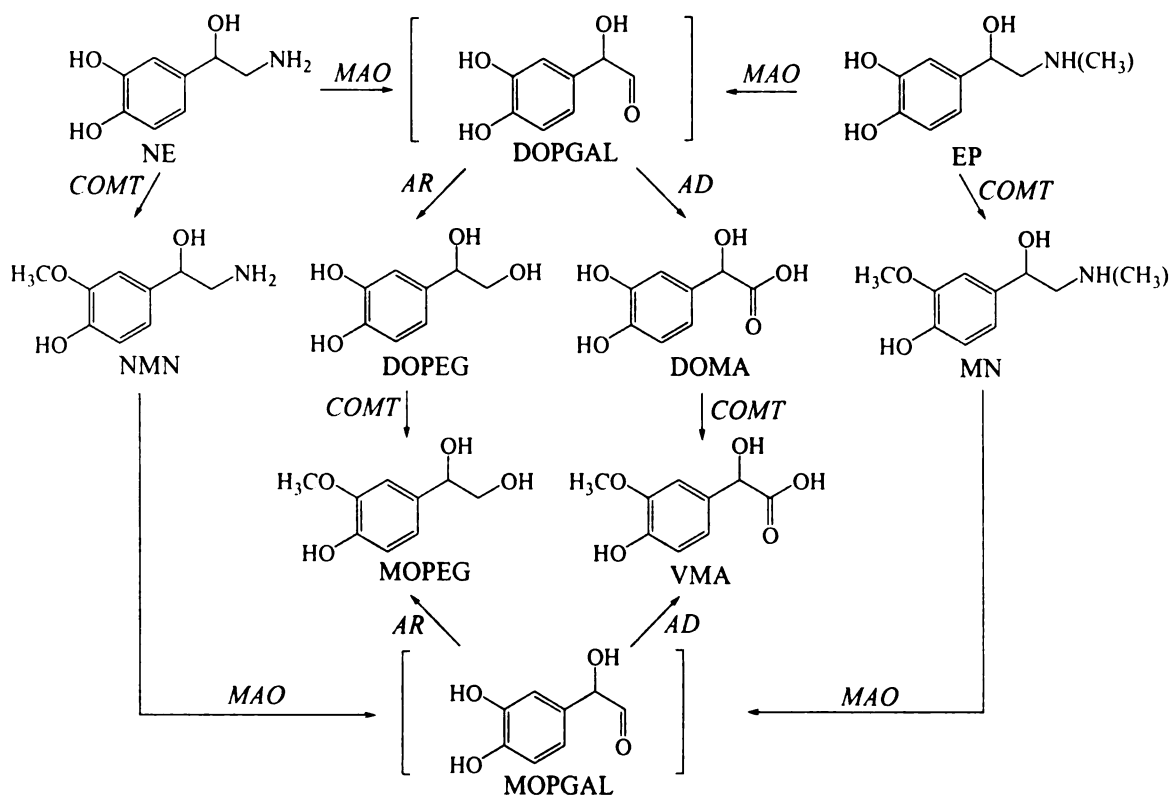
FIA-EC was used to evaluate the performance of diamond as electrodes in the electrochemical detection of catechols and catecholamines. There were many similarities in the detection figures of merit for both diamond and GC electrodes. Linear dynamic ranges from nM to mM levels were seen ($R^2 > 0.99$). The response sensitivity values were in the range of 10 – 30 nA/ μ M while the LOQ values were in the 10 – 60 pg range. Noteworthy is the fact that these figures of merit were obtained for diamond electrodes without any pretreatment while those for GC were obtained only after activation by mechanical polishing. The response precisions for diamond (1 – 3%) were slightly better than those for GC (1 – 5%), and the response stability, at least for NE, was superior for diamond. Diamond electrodes resisted deactivation during 7-h use period and resisted fouling in the presence of BSA more so than GC. While comparable in many respects, diamond electrodes afford advantages over GC for the analysis of catechols and catecholamines in terms of (i) more rapid response stabilization time after detector turn-on, (ii) low background current and peak-to-peak noise, and (iii) good figures of merit without pretreatment. Diamond is attractive for those applications that require continuous measurements over a long period of time and exposure to complex matrices such as those that contain various molecules that cause electrode fouling.

Chapter 4

REVERSED-PHASE HPLC SEPARATION AND AMPEROMETRIC DETECTION OF CATECHOLAMINES AND METABOLITES AT BORON-DOPED DIAMOND THIN-FILM ELECTRODES

4.1. Introduction

Catecholamine neurotransmitters are involved in the control of a variety of regulatory systems, such as psychomotor activity, memory, and hormone secretion.² They are found in the brain, chromaffin cells, sympathetic nerves, and sympathetic ganglia.³ The metabolic pathway of the catecholamines is shown in Figure 4.1.⁷⁷ Two major metabolic processes occur. One involves the oxidation of the aliphatic amine side chain by the enzyme monoamine oxidase (MAO). The aldehyde formed is unstable and may either be reduced to the corresponding alcohol (neutral metabolites) or be further oxidized to an acid (acidic metabolites). The second process involves an O-methylation in the 3-position via the enzyme catechol-O-methyl transferase (COMT).⁵⁸ Since the neurotransmitters are integrated with all bodily systems, changes in catecholamine metabolism are likely to be good markers for various disease states and disorders.⁴



Abbreviations: NE, norepinephrine; DOPGAL, 3,4-dihydroxyphenylglycoaldehyde; EP, epinephrine; NMN, normetanephrine; DOPEG, 3,4-dihydroxyphenylethyleneglycol; DOMA, 3,4-dihydroxymandelic acid; MN, metanephrine; MOPEG, 3-methoxy-4-hydroxyphenylethyleneglycol; VMA, vanillylmandelic acid; MOPGAL, 3-methoxy-4-hydroxyphenylglycoaldehyde; MAO, monoamine oxidase; COMT, catechol-O-methyltransferase; AR, aldehyde reductase; AD, aldehyde dehydrogenase

Figure 4.1. Steps in the metabolism of catecholamines.

In the previous chapter, FIA-EC measurements revealed that diamond is a reliable electrode for the electrochemical detection of catechols and catecholamines. These electroactive analytes are present in complex biological fluids and they all undergo oxidation at similar potentials. Therefore, a separation step is a prerequisite for their detection. Separation and quantification of these analytes in biological fluids provide valuable information on metabolic abnormalities. For example, if an altered level of a

catecholamine is found, the metabolite concentration may be used to confirm the diagnosis of a disease.³ In this chapter, the utility of this new electrode for detecting catecholamines (amperometric mode) in HPLC is demonstrated.

HPLC-EC was originally developed for the analysis of catecholamine neurotransmitters about three decades ago.^{9,10} Since then, the determination of catecholamines and related compounds has remained among the most common applications of the method due to their amenability for electrochemical detection and for their biomedical importance. Some of the related reports on HPLC-EC published recently are presented in Table 4.1.⁷⁸⁻⁸³ The mass limits of detection reported and types of working electrodes used are given in the table.

Table 4.1. Recent publications on HPLC-EC analysis of catecholamines and metabolites.

Ref.	Electrode	Analyte	Detection Limit
[78]	glassy carbon	DOPEG NE	14 pg 40 pg
[79]	glassy carbon	NE EP	4.0 pg 3.2 pg
[80]	multi-wall carbon nanotubes -COOH chemically-modified electrode (MWNT-COOH CME)	NE	0.85 pg
[81]	glassy carbon	NMN MN	183 pg 197 pg
[82]	overoxidized polypyrrole (OPPy) film CME	NE EP	8.5 pg 9.2 pg
[83]	self-assembled <i>n</i> -alkanethiol monolayer (C ₁₀ -SAM)-modified Au	NE	676 pg

In this chapter, the performance of diamond for the determination of catecholamines and metabolites using amperometric detection coupled with HPLC is described. The objectives for the work were: (i) to develop a protocol for separating the catecholamines (NE and EP) and metabolites (DOPEG, VMA, NMN, and MN) by reversed-phase HPLC, (ii) to comprehensively evaluate the analytical detection figures of merit for both microcrystalline and nanocrystalline diamond thin-film electrodes, and (iii) to demonstrate the capability of using this method for catecholamine analysis in a biological sample (e.g., rat plasma).

4.2. Results and Discussion

The reversed-phase HPLC separation of a mixture of catecholamines and related metabolites, coupled with amperometric detection, was investigated. Significant effort was made to achieve an isocratic separation of the components in the mixture. The variables adjusted were the mobile phase composition with the organic modifier (methanol, MeOH), the concentration of the ion-pairing agent (heptanesulfonic acid, HSA), the mobile phase flow rate, and the pH. A satisfactory separation was achieved using 95/5 (v/v) 0.05 M NaH₂PO₄/MeOH, 0.475 mM HSA, pH 2.5, at a flow rate of 0.8 mL/min. A typical chromatogram for a mixture of 20 μM DOPEG, NE, EP, VMA, NMN, and MN is shown in Figure 4.2. The injection volume was 20 μL and the working electrode was a nanocrystalline diamond thin film poised at 950 mV vs. Ag/AgCl for detection.

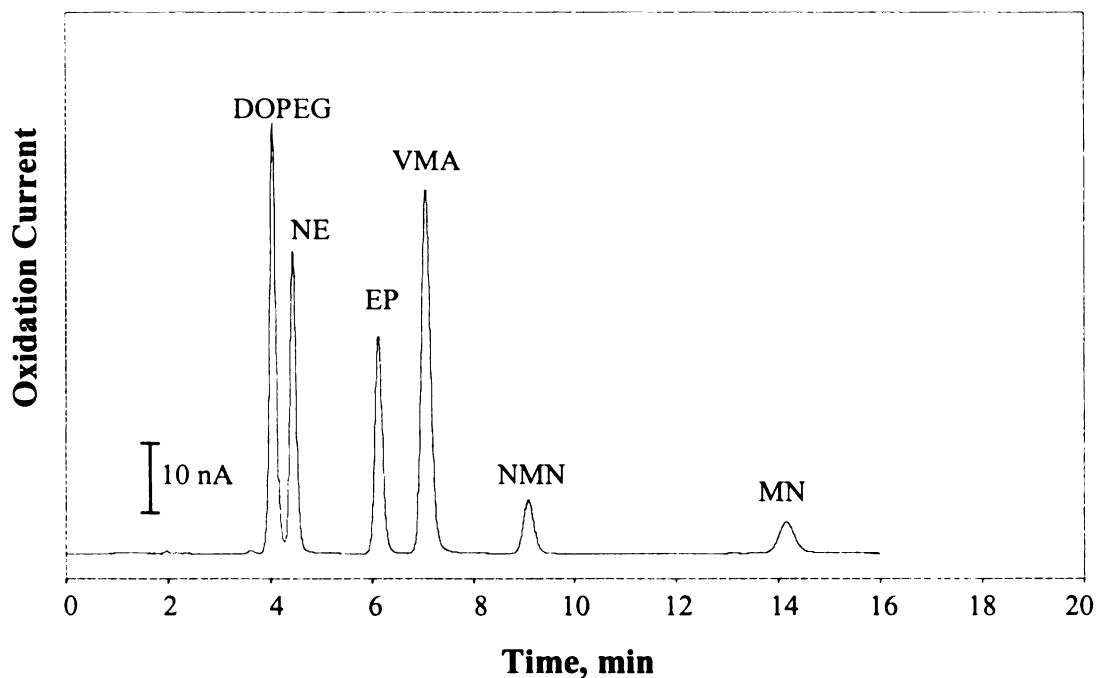


Figure 4.2. Reversed-phase HPLC separation of 20 μM DOPEG, NE, EP, VMA, NMN and MN on a C_{18} column (Alltech Adsorbosphere HS, 5 μm particle size, 4.6 mm x 150 mm). The mobile phase was 95/5 (v/v) 0.05 M $\text{NaH}_2\text{PO}_4/\text{MeOH}$, pH 2.5, 0.475 mM HSA. The working electrode was a nanocrystalline diamond thin film and the detection potential was 950 mV vs. Ag/AgCl. Flow rate = 0.8 mL/min. Injection volume = 20 μL . Electrode geometric area = 0.12 cm^2 .

The background current and peak-to-peak noise were lower for microcrystalline diamond (3.10 nA and 3.95 pA, respectively) than for nanocrystalline diamond (4.30 nA and 4.35 pA, respectively), consistent with the trends observed in Chapter 3. The expected reversed-phase elution order, based on the solute polarities in the presence of the ion-pairing agent, was observed. The dihydroxy analytes (DOPEG, NE, and EP) are retained less strongly on the column than are the 3- O-methyl metabolites (VMA, NMN, and MN). This is because the hydroxy group imparts a greater polar character to the

molecule than does the methoxy group. The ion-pairing agent results in a greater retention of the analytes with the amine side chain, which are extremely polar and hydrophilic, by imparting nonpolar character and hydrophobicity. DOPEG, having an uncharged side-chain does not form an ion-pair, and thus, elutes first. The same can be said about VMA which elutes prior to NMN and MN. EP is less polar than NE due to the presence of the electron-donating methyl group on its aliphatic amine side chain, and is thus retained more strongly. The effect of the presence of methyl on the amine group is two-fold: a reduction of the effective positive charge and a steric hindrance to the electrostatic attraction with the ion-pairing agent. This same reasoning applies to the retention order between MN and NMN. Excellent baseline resolution was achieved for all six solutes with the separation taking a total of 14 min. The calculated retention factors (k) are 1.1, 1.3, 2.1, 2.6, 3.6 and 6.2 for DOPEG, NE, EP, VMA, NMN, and MN, respectively. The peaks are highly symmetric with no tailing. All the peaks are well-resolved with the lowest resolution (R_s) of 1.4 observed between DOPEG and NE. The total number of theoretical plates, N , for the separation is 8210, based on the retention time and peak width of MN, the last eluting solute.

A comprehensive set of detection figures of merit for the catecholamines and metabolites were determined for both nanocrystalline and microcrystalline diamond thin-film electrodes. Calibration curves for all the solutes are shown in Figure 4.3. The detection figures of merit are summarized in Table 4.2.

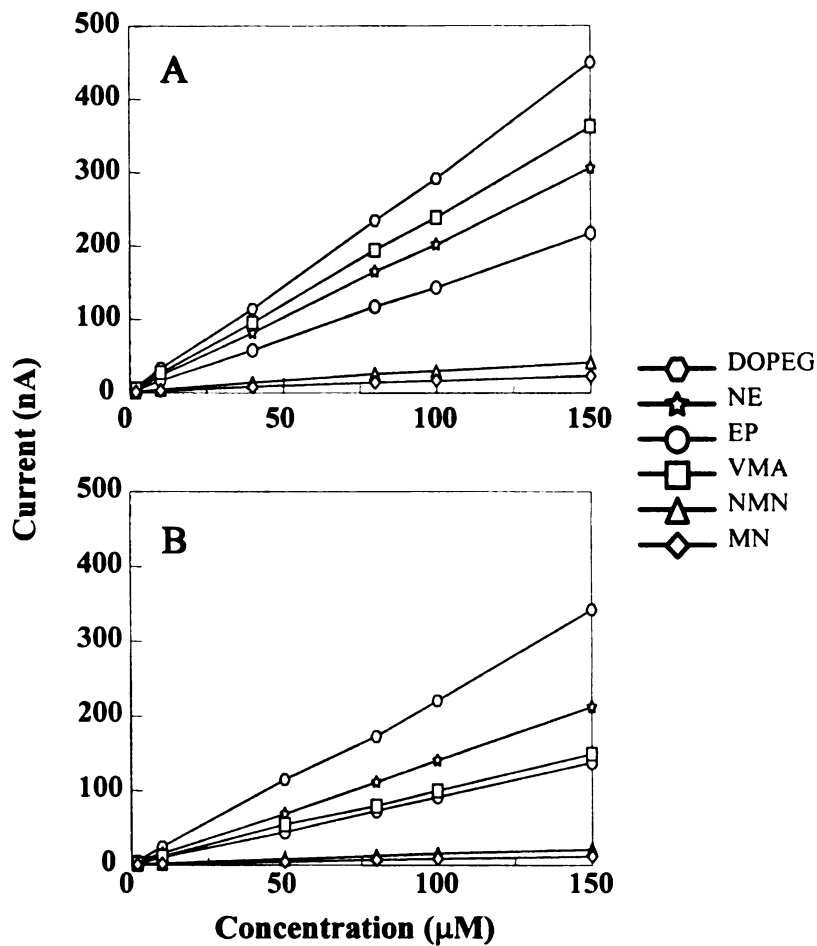


Figure 4.3. Calibration curves obtained at a (A) nanocrystalline and (B) microcrystalline diamond thin-film electrode for a series of mixtures of the catecholamines and metabolites. The separation was carried out in the same conditions as in Figure 4.2. The detection potentials used were 950 mV and 1000 mV vs. Ag/AgCl for A and B, respectively. Injection volume = 20 μL . Electrode geometric area = 0.12 cm^2 .

Table 4.2. Amperometric detection figures of merit for the HPLC-EC analysis of catecholamines and metabolites at nanocrystalline and microcrystalline diamond thin-film electrodes.

Analyte	Response Precision (% RSD)	Linear Dynamic Range	Sensitivity (nA/ μ M)	LOQ at S/N \geq 3
<i>Nanocrystalline Diamond</i>				
DOPEG	0.9	0.003 μ M – 150 μ M	3.3 \pm 0.5	10 pg
NE	1.0	0.01 μ M – 150 μ M	2.0 \pm 0.2	34 pg
EP	1.0	0.01 μ M – 150 μ M	1.4 \pm 0.2	37 pg
VMA	1.6	0.01 μ M – 150 μ M	2.0 \pm 0.6	40 pg
NMN	2.0	0.03 μ M – 150 μ M	0.2 \pm 0.1	110 pg
MN	1.5	0.05 μ M – 150 μ M	0.1 \pm 0.0	197 pg
<i>Microcrystalline Diamond</i>				
DOPEG	5.1	0.007 – 150 μ M	1.7 \pm 0.90	24 pg
NE	5.0	0.03 – 150 μ M	0.8 \pm 0.96	102 pg
EP	5.3	0.03 – 150 μ M	0.5 \pm 0.64	110 pg
VMA	8.8	0.03 – 150 μ M	0.6 \pm 0.57	119 pg
NMN	6.5	0.1 – 150 μ M	0.1 \pm 0.13	366 pg
MN	7.1	0.1 – 150 μ M	0.04 \pm 0.07	1180 pg

Note: The data are based on the response of three electrodes. The sensitivity values are reported at 95% confidence level. The response precision was evaluated based on six injections of a 20 μ M mixture. The calibration curves consisted of at least six points. Experimental conditions are the same as those listed in Figure 4.2.

The linear dynamic range for the solutes is 4 - 6 orders of magnitude ($R^2 > 0.999$) for both diamond types. It should be noted that the maximum concentration of 150 μ M does not represent the upper end of the linear dynamic range but rather just the highest concentration measured. The response precision was determined from six consecutive injections of a 20 μ M mixture of the analytes. The response precision was superior for

nanocrystalline diamond with RSD values of 0.9 – 2.0%. The large response variability for microcrystalline diamond may have been influenced by the column conditions and not the electrode properties. Rigorous column cleaning was performed before the start of the series of measurements with nanocrystalline diamond and may have improved the column performance. For all the solutes, the sensitivity is 2-3 times higher for all the solutes at nanocrystalline than at microcrystalline diamond. The LOQ values for both diamond types are comparable to those of the recently published results for other electrode materials shown in Table 4.1. The LOQ values for nanocrystalline diamond are all at the pg level and are 2-3 times lower than those for microcrystalline diamond. In general, the figures of merit reveal more favorable detection for nanocrystalline diamond, in terms of LOQ, sensitivity and response precision. This is consistent with the larger i_p^{ox} values for nanocrystalline diamond observed in the voltammetric measurements, something that appears to be caused by increased adsorption. Adsorption of catechols is reported to be enhanced when there is a greater fraction of exposed sp^2 -bonded carbon, which is related to smaller grain size.³⁶ However, the superior electrode performance of nanocrystalline diamond in the HPLC-EC is more pronounced than in the FIA-EC measurements.

The usefulness of the HPLC-EC assay for the analysis of a real biological sample was also demonstrated. The catecholamine and metabolite levels in the blood plasma of a laboratory test animal were determined. The work presented herein is a preliminary effort to use HPLC-EC to monitor the circulation levels of catecholamines and metabolites in normotensive and hypertensive rats. The main focus is on the main neurotransmitter released in the sympathetic nerve system, NE, and its four major

metabolites: DOPEG, VMA, NMN, and MN. The rat plasma samples were obtained from Dr. Keith Lookingland of the Department of Pharmacology and Toxicology at Michigan State University. Chromatograms for plasma samples from a normotensive and a hypertensive rat are shown in Figure 4.4. In the hypertensive rat, hypertension was induced by a procedure, introduced by Grollman, known as renal wrap, which involves removing one kidney and then traumatizing the other kidney.⁸⁴

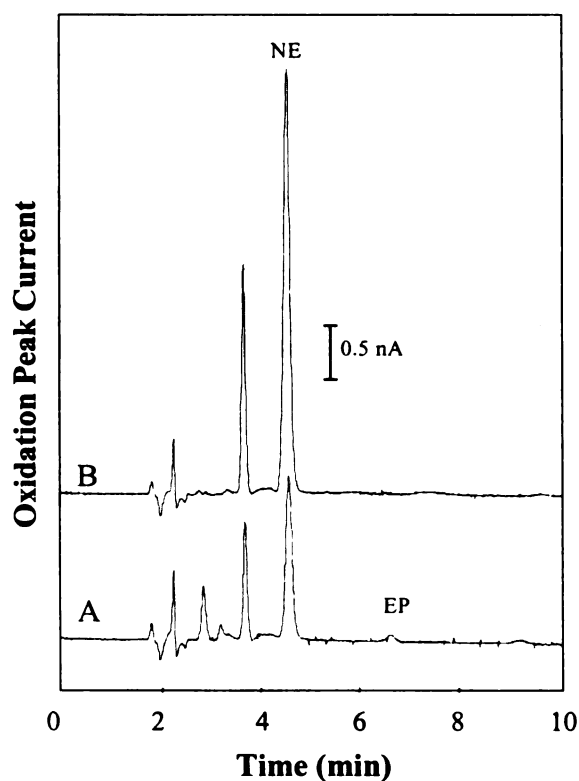


Figure 4.4. Reversed-phase chromatograms for the analysis of plasma samples from (A) a normotensive rat and (B) a hypertensive rat on a C_{18} column (Alltech Adsorbosphere HS, 5 μm particle size, 4.6 mm x 150 mm). The mobile phase was 96/4 (v/v) 0.05 M $\text{NaH}_2\text{PO}_4/\text{MeOH}$, pH 2.5, 0.48 mM HSA. The working electrode was a nanocrystalline diamond thin film and the detection potential was 950 mV vs. Ag/AgCl. Flow rate = 0.8 mL/min. Injection volume = 20 μL . Electrode geometric area = 0.12 cm^2 .

Purification of the plasma samples was accomplished by alumina extraction, a technique that is based on the selective adsorption of catecholamines onto alumina in an alkaline medium. Adsorption occurs by the formation of cyclic complexes, as the vicinal hydroxy groups of the catecholamines are attracted to the alumina matrix. The presence of an amine side chain seems to be unimportant, resulting in the extraction of all catechols, not just catecholamines. The alumina was then washed with water and the catecholamines desorbed by acidification.⁴ The eluted samples were then stored in the freezer (-20 °C) prior to measurement. When the time came for analysis, the sample was thawed and 20 µL was injected onto the reversed-phase column. Elution was performed isocratically with 96/4 (v/v) 0.05 M NaH₂PO₄/MeOH, pH 2.5, 0.48 mM HSA. The chromatogram for the normotensive rat plasma sample revealed seven peaks – the system peak, four peaks with retention times not matching any of the analytes studied, and NE and EP peaks at 4.6 min and 6.7 min, respectively. Peak identification was performed by retention time matching. The chromatogram for the hypertensive rat plasma sample, on the other hand, contained only four peaks – the system peak, two unknown peaks and the NE peak. The identity of the unknown peaks was not determined. Peaks for the metabolites DOPEG, VMA, NMN, and MN were not seen, probably because the sensitivity of the method is not sufficient enough to detect the low concentration of these compounds probably present.

In order to quantitate the NE and EP present, a series of standard solutions was analyzed and calibration curves were constructed from the data. The standard addition method is preferred for complex samples such as this but the quantity of sample was too small to use this method. The NE peak height for the hypertensive plasma sample is

larger than that for the normotensive one indicative of a higher concentration. Although this is the expected result, an uncertainty exists because the NE level of 396 pmol/mL determined for the normotensive sample is much higher than values found in literature, in the low pmol/mL range.^{85,86} There are a couple of possible reasons for this difference. One is that since only two normotensive and two hypertensive samples were measured, there is a possibility that the animals tested were not representative of the population. A second possibility is that the extraction efficiency of 52% used in the calculations is just an estimate based on internal standard measurement (3,4-dihydroxybenzylamine or DHBA). The extraction coefficient is calculated from the known concentration of the internal standard added to the sample before extraction and the concentration determined by the analysis of the extract. This may be a major source of error because the internal standard measurement was not done on the actual sample injected. The EP level of 4.0 pmol/mL for the normotensive sample agrees with the value of 3.76 pmol/mL obtained by the group of Y. Wang.⁸⁶ Other groups have reported plasma EP levels ranging from 0.57 to 0.82 pmol/mL.^{85,87} These variabilities are expected to arise due to differences in the test animal and environmental factors, such as the source, age, diet, weight and condition of the rats, and the time of day, ambient temperature, and sampling site during sample collection.

4.3. Conclusions

The reversed-phase HPLC separation of several catecholamines (NE and EP) and metabolites (DOPEG, VMA, NMN, and MN) was optimized and the performance of microcrystalline and nanocrystalline diamond thin-film electrodes for the amperometric

detection of these analytes was evaluated. Nanocrystalline diamond exhibited good response precision for all analytes with RSD values between 1 and 2%. Microcrystalline diamond exhibited higher RSD values between 5 and 9%. The linear dynamic range was 4 to 6 orders of magnitude for both diamond types. The sensitivity ranged from 0.1 to 4 nA/ μ M for nanocrystalline diamond and from 0.04 to 2 nA/ μ M for microcrystalline diamond. The mass LOQ values ranged from 10 to 100 pg and 20 to 1200 pg, for nanocrystalline and microcrystalline diamond, respectively. In general, nanocrystalline diamond outperformed microcrystalline diamond for the detection of these important compounds. These figures of merit were compared with the recent reports on the HPLC-EC analysis of catechols and catecholamines presented in Table 4.1. The RSD values are comparable to the lowest reported.⁸² The linear dynamic range obtained in this work is the widest. Other groups that used OPPy CME and MWNT-COOH CME reported 3 to 4 orders of magnitude in range.^{80,82} Sensitivity values of 1 to 16 nA/ μ M and 8 to 36 nA/ μ M were reported by S. Zhang⁸² et al and W. Zhang⁸⁰ et al, respectively, indicating that the values obtained in this research needs improvement in this aspect. The LOQ values reported here are comparable to those of the recent works presented in Table 4.1.

A bionalytical application of the HPLC-EC method was demonstrated using rat plasma samples. An attempt was made to correlate hypertension with an increased plasma level of NE. The plasma concentration of epinephrine in a normotensive rat was determined. Further improvement in the sensitivity is needed to extend the usefulness of the detection scheme in the quantitation of biological compounds present in low concentrations.

Chapter 5

SUMMARY AND CONCLUSIONS

The results of the research presented herein demonstrate that catechols and catecholamines can be electrooxidized and quantitatively detected using boron-doped, polycrystalline diamond thin-film electrodes. CV investigations have shown that the electron transfer kinetics are more sluggish on diamond than on GC, presumably due to the absence of adsorption. The redox reaction is faster on nanocrystalline diamond than on microcrystalline diamond and this is attributed to enhanced adsorption due to an increased fraction of exposed sp^2 -bonded carbon. The redox reaction rate for diamond demonstrated pH-dependence, that is, the E_p^{ox} value decreases as the pH increases. Moreover, the rate of electron transfer on diamond show charge discrimination, that is, faster rates are observed for positively-charged than for negatively-charged analytes. This finding is consistent with an electrostatic effect, so the presence of surface oxides is supposed. The surface oxides may have resulted from the wide potential sweeps applied to drive the redox reaction.

The FIA-EC results have indicated that catechols and catecholamines can be detected on diamond electrodes at constant potential. The performance of the diamond electrodes is found to be comparable to that of the more commonly used GC electrode. Diamond exhibited faster stabilization time, and lower background current and peak-to-peak noise compared to GC. The response precision for all three electrode types is good, with average RSD values of 1.8%, 1.5%, and 2.4% for microcrystalline diamond,

nanocrystalline diamond, and GC, respectively. The linear dynamic range, for all three electrode types, is 5 – 6 orders of magnitude, ranging from the nM to the mM level. The sensitivity values for all analytes at the three electrodes are similar, with values ranging from 10 - 30 nA/ μ M. The LOQ values are comparable, all in tens of picograms. The diamond electrodes have demonstrated better response stability. The measured changes in the current response within a 7-h period for microcrystalline and nanocrystalline diamond are 1% and 2%, respectively, while the current decreased by 11% for GC. Diamond exhibits a greater resistance to fouling by interfering biomolecules. The current decrease in the presence of added BSA are 8% for both diamond types and 17% for GC. The performance of diamond thin-film electrodes is comparable to that of GC in terms of linear dynamic range, sensitivity and LOQ. Diamond showed better response stability and lesser susceptibility to fouling. It is important to note that diamond electrodes exhibit optimum performance without any time-consuming and tedious pretreatment steps, as opposed to GC which has to be polished prior to measurement.

The results of the HPLC-EC measurements provide a good starting point for the use of diamond electrodes in physiological research and in routine bioanalytical assays. Response precision is better at nanocrystalline diamond, with RSD values between 1 - 2%, compared to that at microcrystalline diamond, with values between 5 - 9%. The linear dynamic range for the two diamond types is 3 - 5 orders of magnitude. The sensitivity of nanocrystalline diamond, ranging from 0.1 – 3 nA/ μ M, is slightly higher than that of microcrystalline diamond, with values of 0.04 - 2 nA/ μ M. The LOQ values at nanocrystalline diamond are 10 – 200 pg while those at microcrystalline diamond are 20 - 1200 pg. The analytical detection figures of merit for nanocrystalline diamond are

better than that for microcrystalline diamond in the HPLC-EC measurements. This presumably results from adsorption that occurs through the sp^2 -bonded carbon at the grain boundaries of the nanocrystalline diamond surface. The superior performance of nanocrystalline diamond compared to microcrystalline diamond is more pronounced in the HPLC-EC measurements than in the FIA-EC measurements.

The HPLC-EC assay for rat plasma samples showed the presence of NE and EP. However, the calculated NE level is much higher than literature values. Moreover, there is a need to improve the sensitivity of the method to detect the catecholamine metabolites present in low concentrations. This may be accomplished through the manipulation of the diamond film growth conditions to produce nanocrystalline films with a greater fraction of grain boundaries. The use of diamond microelectrodes instead of thin-film electrodes in HPLC-EC may lead to enhanced mass transport and may result in lower mass detection limits. Further improvements in the detection limits and selectivity may be achieved by employing capillary electrophoresis as the separation method. A better knowledge and understanding of the effects of surface modifications such as OPPy-coating,³⁴ electrochemical anodization,⁶⁷ and oxygen termination⁸⁸ on the sensitivity and selectivity for the detection of catecholamines and metabolites are beneficial.

BIBLIOGRAPHY

- (1) In [http://www.lsuagcenter.com/news/July2003/GetGrow/GIGColumn\(PoisonIvivy\)-07-25-03.asp](http://www.lsuagcenter.com/news/July2003/GetGrow/GIGColumn(PoisonIvivy)-07-25-03.asp), accessed August 2004.
- (2) J. Bergquist, A. Sciubisz, A. Kaczor, J. Silberring *J. Neurosci. Methods* **2002**, *113*, 1.
- (3) Z. Yi, P.R. Brown *Biomed. Chromatogr.* **1991**, *5*, 101.
- (4) A.M. Krstulovic *Quantitative Analysis of Catecholamines and Related Compounds*; John Wiley & Sons: New York, 1986.
- (5) N. Unceta, E. Rodriguez, Z.G. de Balugera, C. Sampedro, M.A. Goicolea, S. Barrondo, J. Salles, R. Barrio *Anal. Chim. Acta* **2001**, *444*, 211.
- (6) G.A. Scratchley, A.N. Masoud, S.J. Stohs, D.W. Wingard *J. Chromatogr.*, *169*, 313.
- (7) C.T. Duda, P.T. Kissinger In *Methods in Neurotransmitter and Neuropeptide Research, Part I*; S.H. Parvez, M. Naoi, T. Nagatsu, S. Parvez, Ed.; Elsevier: New York, 1993; Vol. 11.
- (8) J.B. Justice, A.C. Michael, D.B. Neill In *Neuromethods 2: Amines and Their Metabolites*; A. A. Boulton, G.B. Baker, Ed.; Humana Press: New Jersey, 1985.
- (9) P.T. Kissinger, C. Refshauge, R. Dreiling, R.N. Adams *Anal. Lett.* **1973**, *6*, 465.
- (10) C. Refshauge, P.T. Kissinger, R. Dreiling, C.L. Blank, R. Freeman, R.N. Adams *Life Sci.* **1974**, *14*, 311.
- (11) K. Stulik, V. Pacakova In *Quantitative Analysis of Catecholamines and Related Compounds*; A.M. Krstulovic, Ed.; John Wiley and Sons: New York, 1986.
- (12) R.L. McCreery In *Voltammetric Methods in Brain Systems*; A.A. Boulton, G.B. Baker, R.N. Adams, Ed.; Humana Press: New Jersey, 1995, pp 1-26.
- (13) J. Asmussen, D.K Reinhard *Diamond Films Handbook*; Marcel Dekker: New York, 2002.
- (14) P.W. May *Phil. Trans. R. Soc. Lond.* **2000**, *358*, 473.
- (15) M. Iwaki, S. Sato, K. Takahashi, H. Sakairi *Nucl. Instrum. Methods* **1983**, *209*, 1129.

- (16) Yu.V. Pleskov, A.Ya. Sakharova, M.D.Krotova, L.L. Bouilov, B.V. Spitsyn *J. Electroanal. Chem.* **1987**, *228*, 19.
- (17) J. Xu, M.C. Granger, Q. Chen, T.E. Lister, J.W. Strojek, G.M. Swain *Anal. Chem.* **1997**, *69*, 591A.
- (18) G.M. Swain, A.B. Anderson, J.C. Angus *MRS Bull.* **1998**, *23*, 56.
- (19) R. DeClements, G.M. Swain, T. Dallas, M.W. Holtz, R. Herrick III, J.L. Stickney *Langmuir* **1996**, *12*, 6578.
- (20) L. Boonma, T. Yano, D.A. Tryk, K. Hashimoto, A. Fujishima *J. Electrochem. Soc.* **1997**, *144*, L142.
- (21) H.B. Martin, A. Argoitia, U. Landau, A.B. Anderson, J.C. Angus *J. Electrochem. Soc.* **1996**, *143*, L133.
- (22) J. Xu, Q. Chen, G.M. Swain *Anal. Chem.* **1998**, *70*, 3146.
- (23) M.C. Granger, J. Xu, J.W. Strojek, G.M. Swain *Anal. Chim. Acta* **1999**, *397*, 145.
- (24) J. Xu, G.M. Swain *Anal. Chem.* **1998**, *70*, 1502.
- (25) S. Jolley, M. Koppang, T. Jackson, G.M. Swain *Anal. Chem.* **1997**, *69*, 4099.
- (26) M.D. Koppang, M. Witek, J. Blau, G.M. Swain **1999**, *71*, 1188.
- (27) M.A. Witek, G.M. Swain *Anal. Chim. Acta* **2001**, *440*, 119.
- (28) G.W. Muna, N. Tasheva, G.M. Swain *Environ. Sci. Technol.* **2004**, *38*, 3674.
- (29) T.N. Rao, B.H. Loo, B.V. Sarada, C. Terashima, A. Fujishima *Anal. Chem.* **2002**, *74*, 1578.
- (30) T.N. Rao, I. Yagi, T. Miwa, D.A. Tryk, A. Fujishima *Anal. Chem.* **1999**, *71*, 2506.
- (31) E. Popa, Y. Kubota, D.A. Tryk, A. Fujishima *Anal. Chem.* **2000**, *72*, 1724.
- (32) S. Sarada, T.N. Rao, D.A. Tryk, A. Fujishima *Anal. Chem.* **2000**, *72*, 1632.
- (33) J. Cvacka, V. Quaiserova, J. Park, Y. Show, A. Muck, Jr., G.M. Swain *Anal. Chem.* **2003**, *75*, 2678.
- (34) H. Olivia, B.V. Sarada, D. Shin, T.N. Rao, A. Fujishima *Analyst* **2002**, *127*, 1572.
- (35) *SciFinder Scholar*; Am. Chem. Soc.: Columbus, 2002.
- (36) Y. Show, M.A. Witek, P. Sonthalia, G.M. Swain *Chem. Mater.* **2003**, *15*, 879.

- (37) L. Bergman, R.J. Nemanich *J. Appl. Phys.* **1995**, *78*, 6709.
- (38) J. Birrell, J.E. Gerbi, O. Auciello, J.M. Gibson, J. Johnson, J.A. Carlisle *Diam. Relat. Mater.* **2005**, *14*, 86.
- (39) A.C. Ferrari, J. Robertson *Phys. Rev. B* **2001**, *63*, 121405.
- (40) D.M. Gruen, A.R. Krauss, C.D. Zuiker, R. Csencsits, L.T. Terminello, J.A. Carlisle, I. Jimenez, D.G.J. Sutherland, D.K. Shu, W. Tong, F. Himpsel *J. Appl. Phys. Lett.* **1996**, *68*, 1640.
- (41) L. Ostrovskaya, V. Perevertailo, V. Ralchenko, A. Dementjev, O. Longinova *Diam. Relat. Mater.* **2002**, *11*, 845.
- (42) M.C. Granger, G. M. Swain *J. Electrochem. Soc.* **1999**, *146*, 4551.
- (43) P. Chen, R.L. McCreery *Anal. Chem.* **1996**, *68*, 3958.
- (44) C. Levy-Clement, F. Zenia, N. Awa Nadao, A. Deneuille *New Diamond Frontier Carbon Technol.* **1999**, *9*, 189.
- (45) R. Keller, I. Mefford, A. Oke, E. Strobe, J. Conti, R.M. Wightman, P. Plotsky, R.N. Adams *Modern Pharm.* **1977**, *10*, 761.
- (46) P.S. Cahill, J.M. Finnegan, G.E. Mickelson, E.R. Travis, R.M. Wightman *Anal. Chem.* **1996**, *68*, 3180.
- (47) D. Pletcher *A First Course in Electrode Processes*; Alresford Press: England, 1991.
- (48) P.T. Kissinger, W.R. Heineman *J. Chem. Ed.* **1983**, *60*, 702.
- (49) J. Wang *Analytical Electrochemistry*, 2nd ed.; Wiley: New York, 2000.
- (50) M.L.A.V. Heien, M.A. Johnson, R.M. Wightman *Anal. Chem.* **2004**, *76*, 5697.
- (51) R. L. McCreery In *Voltammetric Methods in Brain Systems*; A.A. Boulton, G.B. Baker, R.N. Adams, Ed.; Humana Press: New Jersey, 1995, pp 1-26.
- (52) S.H. Duvall, R.L. McCreery *J. Am. Chem. Soc.* **2000**, *122*, 6759.
- (53) G.N. Kamau, W.S. Willis, J.F. Rusling *Anal. Chem.* **1985**, *57*, 545.
- (54) P.L. Runnels, J.D. Joseph, M.J. Logman, R.M. Wightman *Anal. Chem.* **1999**, *71*, 2782.
- (55) M.R. Deakin, P.M. Kovach, K.J. Stutts, R. M. Wightman *Anal. Chem.* **1986**, *58*, 1474.

- (56) M.R. Deakin, K.J. Stutts, R.M. Wightman *J. Electroanal. Chem.* **1985**, *182*, 113.
- (57) D.C.S. Tse, R.L. McCreery, R.N. Adams *J. Med. Chem.* **1976**, *19*, 37.
- (58) A.W. Sternson, R. McCreery, B. Feinberg, R.N. Adams *J. Electroanal. Chem. Interfacial Electrochem.* **1973**, *46*, 313.
- (59) M.D. Hawley, S.V. Tatawadi, S. Piekarski, R.N. Adams *J. Am. Chem. Soc.* **1967**, *89*, 447.
- (60) A.J. Bard, L.R. Faulkner *Electrochemical Methods: Fundamentals and Applications*, 2nd ed.; John Wiley and Sons, Inc.: New York, 2001.
- (61) E. Laviron *J. Electroanal. Chem.* **1984**, *164*, 213.
- (62) M.R. Deakin, R.M. Wightman *J. Electroanal. Chem.* **1986**, *206*, 167.
- (63) K.T. Kawagoe, P.A. Garris, R.M. Wightman *J. Electroanal. Chem.* **1993**, *359*, 193.
- (64) S.H. Duvall, R.L. McCreery *Anal. Chem.* **1999**, *71*, 4594.
- (65) C.D. Allred, R.L. McCreery *Anal. Chem.* **1992**, *64*, 444.
- (66) M.C. Granger, M. Witek, J. Xu, J. Wang, M. Hupert, A. Hanks, M.D. Koppang, J.E. Butler, G. Lucazeau, M. Mermoux, J.W. Strojek, G.M. Swain *Anal. Chem.* **2000**, *72*, 3793.
- (67) E. Popa, H. Notsu, T. Miwa, D.A. Tryk, A. Fujishima *Electrochem. Solid-State Lett.* **1999**, *2*, 49.
- (68) I. Duo, C. Levy-Clement, A. Fujishima, C. Comninellis *J. Appl. Electrochem.* **2004**, *34*, 935.
- (69) J. Ruzicka, E.H. Hansen *Anal. Chim. Acta* **1975**, *78*, 145.
- (70) J. Ruzicka, E.H. Hansen *Flow Injection Analysis*, 2nd ed.; J. Wiley: New York, 1988.
- (71) E.H. Hansen, J. Ruzicka *J. Chem. Ed.* **1979**, *56*, 677.
- (72) J. Ruzicka, E.H. Hansen *Anal. Chem.* **2000**, *72*, 212A.
- (73) In <http://www.lachatstruments.com/products/qcfia/FIAPrimer.asp>., accessed August 2004.
- (74) W.R. Lacourse *Pulsed Electrochemical Detection in High Performance Liquid Chromatography*; Wiley: New York.

- (75) G. Dryhurst *NATO ASI Ser., Ser. A* **1994**, 267, 171.
- (76) In http://www.thinkquest.org/library/site_sum.html?tname=C0115080&url=C0115080/%3fc=plasma, accessed August 2004.
- (77) G. Eisenhofer, T. Huynh, M. Hiroi, K. Pacak *Rev. Endocr. Metab. Disord.* **2001**, 2, 297.
- (78) E. Sastre, A. Nicolay, B. Bruguerolle, H. Portugal *J. Chromatogr. B* **2004**, 801, 205.
- (79) J. Ueyama, K. Kitaichi, M. Iwase, K. Takagi, K. Takagi, T. Hasegawa *J. Chromatogr. B* **2003**, 798, 35.
- (80) W. Zhang, Y. Xie, S. Ai, F. Wan, J. Wang, J. Jin *J. Chromatogr. B* **2003**, 791, 217.
- (81) K. Vuorensola, H. Siren, U. Karjalainen *J. Chromatogr. B* **2003**, 2003, 277.
- (82) S. Zhang, Q. Xu, W. Zhang, L. Jin, J. Jin *Anal. Chim. Acta* **2001**, 427, 45.
- (83) Z. Liu, J. Li, S. Dong, E. Wang *Anal. Chem.* **1996**, 68, 2432.
- (84) A. Grollman *Proc. Soc. Exp. Biol. Med.* **1944**, 57, 102.
- (85) K. Takezawa, M. Tsunoda, N. Watanabe, K. Imai *Anal. Chem.* **2000**, 72, 4009.
- (86) Y. Wang, D.S. Fice, K.F. Yeung *J. Pharm. Biomed. Anal.* **1999**, 21, 519.
- (87) J.W.M. Lenders, R. Kvetnansky, K. Pacak, D.S. Goldstein, I.J. Kopin, G. Eisenhofer *J. Pharmacol. Exp. Ther.* **1993**, 266, 288.
- (88) I. Yagi, H. Notsu, T. Kondo, D.A. Tryk, A. Fujishima *J. Electroanal. Chem.*, 473, 173.

MICHIGAN STATE UNIVERSITY LIBRARIES



3 1293 02732 5087